Nucl. Fusion **47** (2007) S501–S520 doi:10.1088/0029-5515/47/10/S02

Conference summary: progress in experiments on innovative concepts, confinement and performance

J. Paméla[1] **and R. Kamendje**[2,3,a]

[1] EFDA, Close Support Unit–Garching, Boltzmannstrasse 2, D-85748 Garching, Germany
[2] EFDA-JET, Culham Science Centre, Abingdon, Oxfordshire OX14 3DB, UK
[3] Institut für Theoretische Physik-Computational Physics, Technische Universität Graz, Petersgasse 16, A-8010 Graz, Austria

E-mail: richard.kamendje@jet.efda.org

Received 17 January 2007, accepted for publication 7 June 2007
Published 17 September 2007
Online at stacks.iop.org/NF/47/S501

Abstract
This paper summarizes the results presented at the 21st IAEA Fusion Energy Conference in the areas of innovative confinement concepts, magnetic confinement experiments and performance.

PACS numbers: 52.25.Fi, 52.25.Vy, 52.30.−q, 52.35.Qz, 52.35.Ra, 52.50.−b, 52.50.Gj, 52.50.Nr, 52.50.Qt, 52.50.Sw, 52.55.−s, 52.55.Fa, 52.55.Hc, 52.55.Ip, 52.55.Jd, 52.55.Lf, 52.55.Di, 52.55.Rk

(Some figures in this article are in colour only in the electronic version)

1. Introduction

At this conference 14 papers were presented on innovative confinement or confinement-related concepts, 90 on confinement experiments with a focus on scenario performance, transport and confinement properties. The highlights include considerable progress on the physics of zonal flows, the development of plasma scenarios toward more ITER-relevant parameters (rotation, collisionality ν^*, T_e/T_i, Greenwald fraction n/n_G), the extension of the operational space of tokamak hybrid regimes towards a region of improved fusion performance, the prediction of significant peaking of the density profile in ITER and the demonstration of a plasma regime with a super dense core in the stellarator LHD.

2. Innovative confinement and confinement-related concepts

In this session, experiments, numerical studies and new ideas were reported, of which a few examples are presented here.

2.1. Innovative ideas

New ideas include the X-divertor concept [1] proposed to address the core confinement and stability problems caused by the extremely high core radiation fractions (∼70–90%) requirements in tokamak fusion reactors with heating powers considerably larger than in ITER [2] due to the limited thermal power handling capability of standard divertors. The underlying features of X-divertors reside in the effect of flaring field lines just before they hit the divertor plates by using small modular non-axisymmetric coils (see figure 1), thereby increasing the plasma wetted area by a factor of up to 2

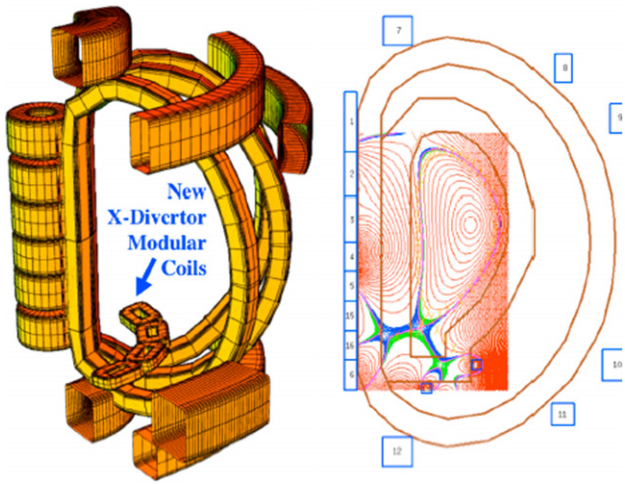

Figure 1. X-divertors coils and CREST equilibrium as proposed to address the core confinement and stability problems caused by the extremely high core radiation fractions requirements in tokamak fusion reactors with heating powers considerably larger than in ITER.

[a] Author to whom any correspondence should be addressed.

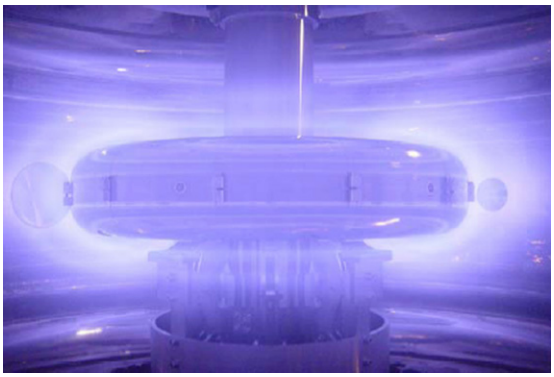

Figure 2. First plasma produced by the RT-1 experiment using ECH with an 8.2 GHz microwave. The equilibrium state produced by this device simulates Jupiter's magnetosphere.

for a given degree of sensitivity to plasma motion. A full engineering and physics study would be welcome to assess this novel idea.

As a way to optimize the magnetic confinement concept in view of fusion reactor relevance (steady-state and high $\beta = 2\mu_0\langle p\rangle/B^2$, B: magnetic field, $\langle p\rangle$: averaged plasma pressure) the EPSILON project—closed rippled magnetic trap without rotational transform and with poloidal pseudo symmetry to provide high β operation; in practice, two or more crimped mirror traps closed with curvilinear elements—is being proposed [3]. The basic difference between the EPSILON project and Kadomtsev's original idea of magnetic traps with rippled magnetic field [4] is the magnetohydrodynamic (MHD) stability and plasma cleaning to be provided by axially symmetrical divertors located along the mirror traps with a zero magnetic field at the separatrix.

2.2. Innovative confinement experiments

The theory of self-organized states in flowing plasmas [5] predicts that the hydrodynamic pressure in a fast plasma flow can balance the thermal pressure (Bernoulli's law), creating a relaxed state with an appreciably high β value. The novel ring trap 1 (RT-1) experiment [6] aims at exploring various effects of flow-field couplings and ways to advanced-fuel fusion (D–^{3}He) that requires a very high β value. RT-1 confines plasmas in a magnetosphere-like field produced by a superconducting magnet levitated in a vacuum chamber. The first plasma experiment on RT-1 was performed in January 2006, with the plasma produced by 1.5 kW electron cyclotron heating (ECH) (figure 2) and a pulse duration of 1 s. The superconductor ring was levitated about 30 mm over the lifter.

Unlike most other approaches to magnetic confinement in which stability requires average good curvature and magnetic shear, MHD stability in a magnetic dipole derives from plasma compressibility. Dipole confinement is determined by the MHD prediction that a dipole-confined plasma remains stable below a critical pressure gradient. First production of high β plasma confined by a laboratory superconducting dipole in the levitated dipole experiment (LDX—a new research facility that is investigating plasma confinement and stability in a dipole magnetic field configuration as a possible catalyzed D–D fusion power source that would avoid the burning of tritium) has been reported [7]. Steady equilibrium for longer than 10 s using neutral gas fuelling and electron cyclotron resonance heating (ECRH) has been demonstrated. It is anticipated that levitation will significantly improve confinement, and the balance of heating and fuelling sources with cross-field transport will set equilibrium plasma profiles.

Magnetic confinement systems free of transformer action or poloidal field coils are attractive for reactors. The new steady-state inductive helicity injection method of the HIT-SI device [8] has begun operation and, for the first time, a steady-state spheromak with n (toroidal mode number) $= 0$ symmetry, about 12 kA of toroidal current has been formed and sustained through non-linear relaxation using about only 3 MW of power [9]. However, the energy confinement time of the spheromak has not been understood yet and is not increased when the power is kept on for a longer time.

The field-reversed configuration has a number of advantages in view of a fusion reactor. It has a toroidal plasma current, but no toroidal magnetic field, leading to a simply connected geometry, high plasma β, a natural divertor structure and possible separation of formation and fusion burn regions. However, plasma stability with respect to low n MHD modes remains a serious issue for field-reversed configurations. Encouragingly, studies of free-boundary field-reversed configurations with improved stability in the magnetic reconnection experiment [10] show that the destructive $n = 1$ tilt instability could be eliminated by forming very oblate plasmas or stabilizing the plasma with a copper centre-column. Improved stability and confinement in a self-organized high β (over 85%) spherical-torus-like field-reversed configuration has also been achieved in the translation, confinement and sustainment (TCS) experiment by highly super Alfvénic translation of a spheromak-like plasmoid [11].

3. Progress on mirror experiments

Modern axially symmetric magnetic mirror traps are among the simplest magnetic plasma confinement devices in addition to their intrinsic capability of steady-state operation. In recent years substantial progress in the suppression of longitudinal heat losses to the end walls via electron thermal conductivity [12], in the stabilization of plasma MHD instabilities [13, 14] and in the understanding of key physical phenomena determining plasma confinement and heating [15] in mirror systems have contributed to laying the foundation for their fusion reactor relevance.

Success achieved in the multi mirror linear trap GOL-3 in heating and confinement of dense plasmas ($T_e \sim T_i \sim 2$–4 keV, $n \sim 10^{21}$ m^{-3}, $nT\tau \sim 10^{18}$ m^{-3} s keV, T_e: electron temperature, T_i: ion temperature, n: particle density, τ: energy confinement time) [16] combined with the upgrade under consideration provide this facility with a valuable potential for testing plasma facing components at high heat fluxes of hot electron plasmas [17]. The gas dynamic trap GDT experiment is being proposed as a powerful 14 MeV neutron source with low power and tritium consumption (60 MW and 150 g y^{-1}, respectively) and appropriate neutron flux density (2 MW m^{-2} or 10^{14} neutrons cm^{-2} s^{-1}) and testing zone area

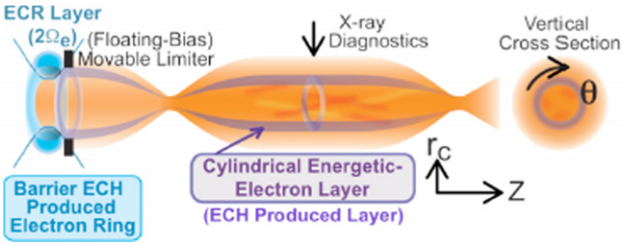

Figure 3. The experimental configuration for radial transport barrier formation by means of off-axis ECH in GAMMA 10.

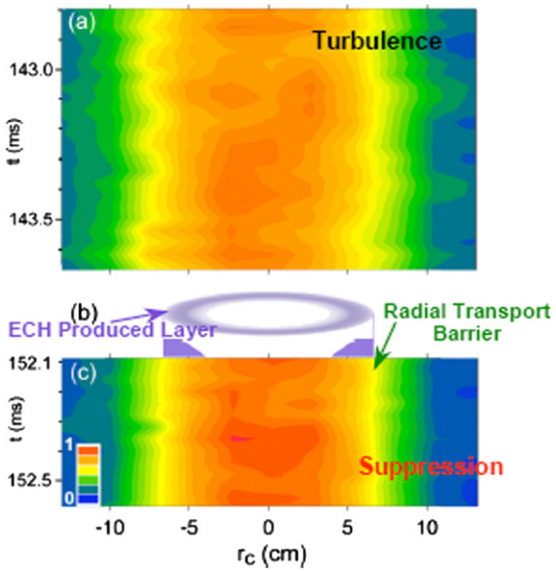

Figure 4. GAMMA 10: contours of central-cell x-ray brightness (*a*) with and (*c*) without cylindrically shaped energetic-electron layer formation due to off-axis barrier by ECH (*b*). Hot-coloured areas show higher plasma pressure locations. Strong turbulence with vortex-like structures continue to exist at $r_c < 4$ cm in (*a*) and (*c*). However, a region of considerable suppression is observed in (*c*) in the energetic-electron layer ($5 < r_c < 7$ cm) and the outer surrounding cylindrical layer ($7 \leqslant r_c < 10$ cm) (intensity $I \propto n_e n_i T_e^{2.3}$).

(of the order of 1 m^2) for fusion reactor-relevant material testing [17].

Significant progress in potential formation and radial transport barrier production for turbulence suppression and improved confinement in the tandem mirror GAMMA 10 was reported [18]. Figure 3 shows the experimental configuration used to externally actively control, for the first time by means of off-axis ECH generated cylindrical $E \times B$ sheared flow, an internal energy transport barrier formation. Intermittent turbulent vortex structures and effects of their suppression by strongly sheared plasma rotation were observed [19]. Here, the suppression of turbulence and the associated significant reduction in cross-field transport (see figure 4) show behaviours that are similar to those seen during transitions from low to high confinement regimes in tokamaks, with improved core plasma confinement [20]. Central-cell ECH (250 kW) is used to raise T_{e0} (central electron temperature) from 70 to 750 eV together with $T_{i\perp 0} = 6.5$ keV, and $T_{i\parallel 0} = 2.5$ keV.

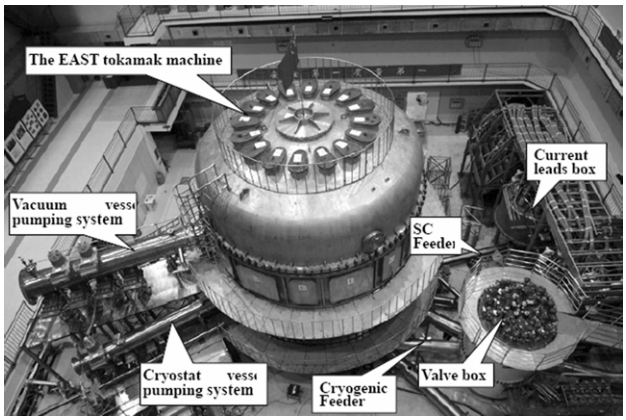

Figure 5. The EAST superconducting tokamak with the vacuum pumping systems, the feeders and the valve box.

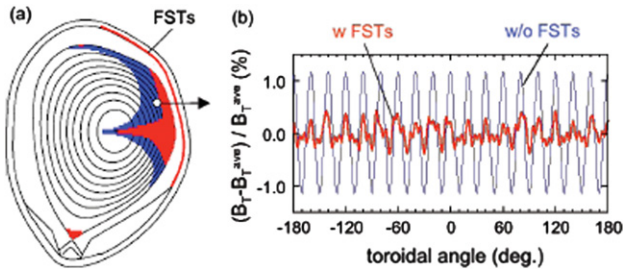

Figure 6. (*a*) Poloidal location of the installed ferritic steel tiles (FSTs) in JT-60U (red line), together with indications of the extent of the quasi-ripple well regions for the cases with no FSTs (blue) and with installed FSTs (red), in the toroidal angle of 0°–20° and at $B_T = 1.86$ T. (*b*) Toroidal variation of the toroidal magnetic field strength at $R = 4.2$ m and $Z = 0.6$ m (circle in (*a*)) for the cases with no FSTs (blue) and with installed FSTs (red).

4. Achievements on toroidal magnetic fusion devices

4.1. Main recent hardware improvements on tokamaks

Improvements with different emphasis on several tokamaks across the world were reported. One of the highlights was the completion and start of the EAST tokamak (see figure 5). EAST is now the largest operating fully superconducting divertor tokamak with a double null capability. Its nominal parameters are as follows: plasma major radius $R = 1.75$ m, plasma minor radius $a = 0.4$ m, toroidal magnetic field $B_T = 3.5$ T, plasma current $I_p = 1$ MA and pulse length 1–1000 s. The first plasma on EAST was obtained on 26 September 2006 and a discharge duration of up to 4.5 s had already been achieved at the time of the conference [21]. EAST will be devoted to the investigation of both the physics and the technology of a steady-state advanced tokamak as well as power and particle handling under steady-state operation conditions.

In order to reduce toroidal magnetic field ripple in JT-60U ferritic steel tiles have been installed on the low field side inside the vacuum vessel in place of graphite tiles (see figure 6(*a*)), and cover ~10% of the vacuum vessel surface [22]. The toroidal field ripple is consequently reduced by a factor of about 4 at $R = 4.2$ m and $Z = 0.6$ m in the case of a toroidal magnetic field of 1.86 T as shown in figure 6(*b*). Monte-Carlo simulations considering fully 3D magnetic field structure

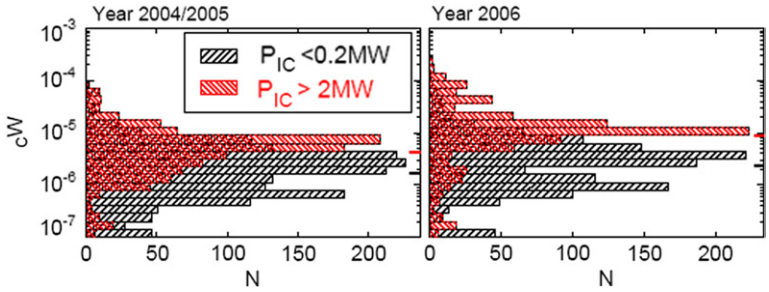

Figure 7. Distributions of tungsten edge concentration in ASDEX Upgrade with (red or from left to right shaded areas) and without (black or from right to left shaded areas) considerable ICRF heating for the campaign 2006 with tungsten limiters in comparison with two previous campaigns with graphite limiters. Bars on the right-hand side give mean values. Without ICRF the distributions are very similar, while with ICRF the mean value of tungsten concentration is increased by about a factor of 5 in the 2006 campaign and only by a factor of 2 in the previous campaigns.

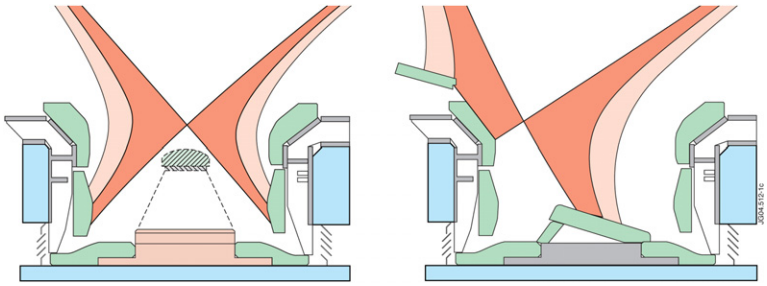

Figure 8. Magnetic configurations in the previous (left) and the present (right) JET divertor. The present divertor (Mk-II-HD) allows the strike points to be shifted inwards, to form configurations with high, ITER-like triangularity.

using the F3D OFMC code indicate that the total absorbed power increases by ∼30% at $B_T < 2$ T for the large volume configuration close to the wall, which had so far suffered from the large toroidal field ripple [23], leading to smaller required neutral beam (NB) units for a given normalized beta, $\beta_N = \beta/(I_p/aB)$, better flexibility in neutral beam injection (NBI) combination and better flexibility of the torque profile. In addition, the effects of the installation of the ferritic steel tiles on toroidal rotation and confinement have been clearly observed [24, 25]. The reduction of the radial electric field attributed to the decrease in the fast ion loss with the ferritic steel tiles is believed to slow down the ctr-rotation at the plasma edge which so far was characteristic of JT-60U (see also section 4.5.1).

High-Z materials are interesting candidates for plasma facing components in future fusion devices in view of the high erosion of low-Z materials and, in particular, tritium retention in carbon and the destruction of graphite under neutron bombardment [26, 27]. In recent years ASDEX Upgrade has been investigating the potential of tungsten (W) as a first wall material [28]. The main risk in using tungsten is a strong central radiation loss and, therefore, the tungsten concentration has to be kept below a level of about 10^{-4}. Since the last IAEA 2004 the coverage of the ASDEX Upgrade vessel interior with tungsten was further extended up to 85% (36 m^2) with the coating of the poloidal limiters at the low field side which receive the highest load in the main chamber [29]. The complete coverage is being performed in the present shut-down of ASDEX Upgrade, namely the 200 μm tungsten coatings on graphite of the remaining lower divertor targets by vacuum plasma spray. It was reported that with increasing tungsten coverage a clear reduction of the carbon concentration was seen, which is, however, less than proportional to area reduction [30]. Moreover, the increase of tungsten-coated areas is also reflected in an increase of the tungsten content. However, the W concentration could be kept in the range or below 10^{-5} over a broad range of discharge scenarios but has been shown to be related to the ion cyclotron heating power which strongly increases the limiter tungsten source, as indicated in figure 7. This figure shows the distribution of W concentrations with (red/grey) and without (black) considerable ICRF heating, taken during time intervals of sufficiently constant plasma parameters for the last campaign with the new W-based limiters and the two previous campaigns with only the central column as the major tungsten source in the main chamber. Mean values are indicated as bars of the same colour. Without ICRF the distributions are very similar, while with ICRF the mean value of W concentration is increased by about a factor of 5 in the last campaign and only by a factor of 2 in the previous campaigns. It is hence found that ICRF strongly increases the limiter W-source.

The JET tokamak has also undergone significant hardware improvements including upgrading of its divertor, heating systems and diagnostics [31]. The new Mk-II-HD (high delta) JET divertor, in replacement to the Mk-II-GB (gas box) divertor (see figure 8), allows high power operation (40 MW power handling capability) with a more ITER-like, high-triangularity plasma shape (see figure 9) at high plasma current (up to 3.5–4 MA). The 15 new or upgraded diagnostics on JET include core diagnostics (such as a new charge exchange recombination spectroscopy system with a time resolution of 10 ms, a new high resolution Thomson scattering system, an X-mode reflectometer making use of new, low-loss wave guides), burning plasma diagnostic (a new time-of-flight

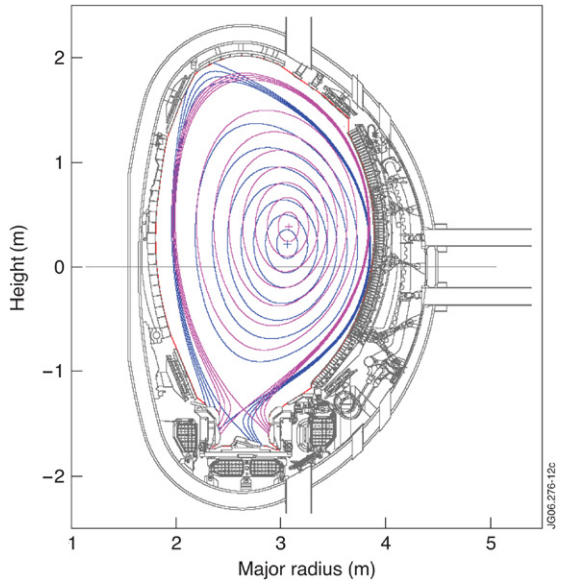

Figure 9. Comparison of a low and a high-triangularity configuration in JET with the new Mk-II-HD divertor.

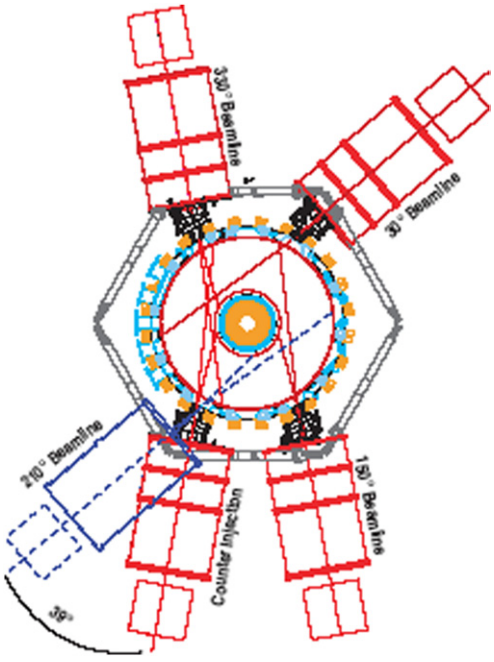

Figure 10. Re-configuration of the NB system on DIII-D by reorientation of one of the beamlines (from red to blue on the picture) now allows 5 MW counter-NBI and 12.5 MW co-NBI and provides fine control of plasma rotation.

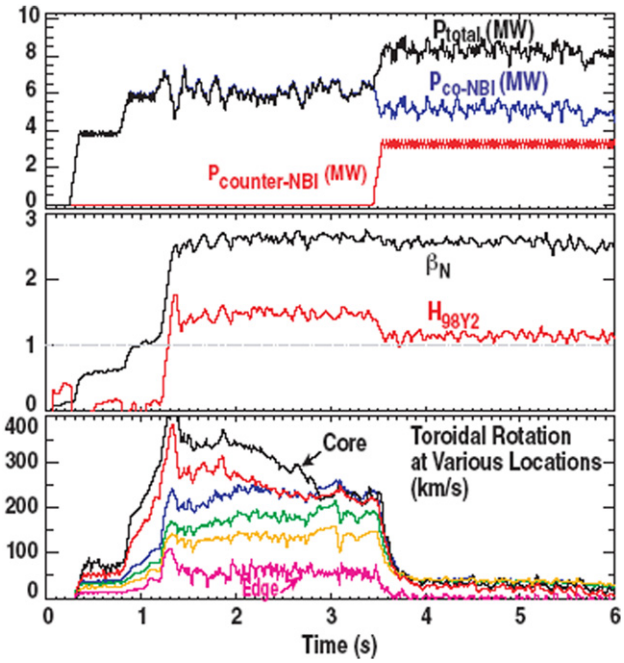

Figure 11. Demonstration of plasma rotation control following the re-configuration of the NB system on DIII-D.

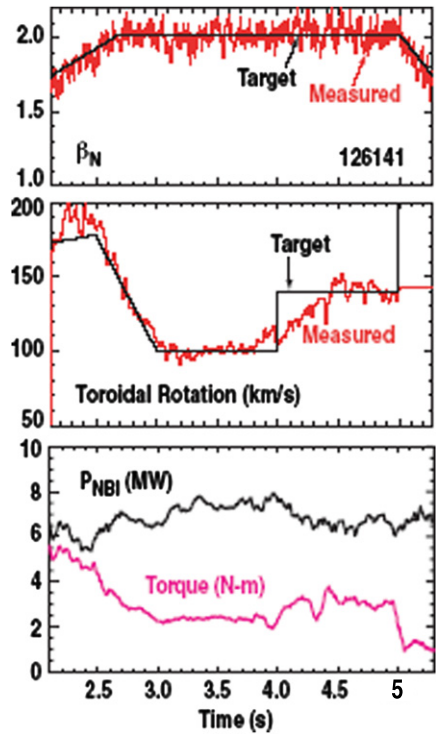

Figure 12. Demonstration of simultaneous feedback control of β_N and toroidal rotation following the re-configuration of the NB system on DIII-D. Feedback control ends at $t = 5.0$ s.

neutron spectrometer for 2.45 MeV neutrons, an upgraded magnet proton recoil for 2.5 and 14 MeV neutrons, and scintillator probes and Faraday cups to measure alpha particle losses), edge and wall diagnostics and protection (a new divertor bolometer, a new wide-angle infra red camera, new quartz microbalances in the divertor, ex-vessel magnetics (located outside the vacuum vessel), new halo current sensors and a new disruption mitigation valve).

To enable tests of the importance of plasma rotation on transport and stability, the NB system on the DIII-D tokamak has recently been reconfigured (see figure 10) to provide up to 5 MW of counter-NB injected power along with 12 MW of co-NB injected power, thereby providing a powerful tool for controlling plasma rotation (see figure 11). Figure 12 illustrates a subsequent demonstration of simultaneous feedback control of β_N and toroidal rotation [32].

4.2. Progress on ITER-relevant tokamak plasma scenarios

Reports from several devices have mentioned substantial progress in improving plasma scenarios to higher confinement and performance. Three main operating scenarios are being investigated for ITER: the inductive H-mode scenario with Type I edge localized modes (ELMs) (commonly referred to as the Type I ELMy H-mode) featuring an edge transport barrier; the hybrid scenario which essentially differs from the ELMy H-mode scenario by the shape of the safety factor q profile and q at the centre being above unity, and its long pulse capability; the advanced tokamak scenario with reversed magnetic shear ($s = r(\mathrm{d}q/\mathrm{d}r)/q$), internal transport barrier (ITB) and steady-state capability.

Tokamak discharge scenario optimization and its extrapolation toward ITER have been one of the highlights of this conference. In particular, ASDEX Upgrade, DIII-D, JET and JT-60U have expanded the envelope of viable, ITER-relevant stationary operation, highlighted by the demonstration of sustained operation of high β_N (~2–4) at high performance ($H_{98}(y,2) > 1$, $H_{98}(y,2)$: confinement enhancement factor over the ITER Physics Basic 1998 $(y,2)$ energy confinement scaling, commonly referred to as IPB98$(y,2)$ where y refers to the ELMy H-mode and 2 to a specific dataset used to derive the scaling [33]) in various experimental conditions and over a wide range of safety factors q_{95} (3–5) and normalized collisionality, ν^* = connection length/(trapped particle mean-free path).

4.2.1. The ITER baseline scenario (Type I ELMy H-mode). The ITER baseline scenario, chosen to meet the Q (ratio of fusion power to input power) = 10 objective, is the Type I ELMy H-mode. In view of the high power loadings that would result from the Type I ELMs in ITER, it is essential to develop this baseline scenario towards one with more benign ELMs. Several tokamak experiments have contributed to the progress in the research in that area. In particular, on DIII-D, a potential solution to ELM control has emerged from experiments which utilize edge resonant magnetic perturbations (RMPs) with $n = 3$ symmetry to completely eliminate ELMs [34, 35], and recent experiments [32] have extended this capability to include complete ELM suppression in a plasma shape similar to the ITER baseline shape and at a pedestal collisionality comparable to that anticipated in ITER (see figure 13).

Type III ELMs, such as those obtained with impurity injection, are usually accompanied by a reduction in confinement which becomes marginal when extrapolated to ITER and requires further qualification. A stationary regime with high confinement and intrinsically benign ELMs, which closely resembles the Type II ELMy regime of ASDEX Upgrade, has been produced on JET (see figure 14) [31]. This was achieved by matching the plasma shape closely to the quasidouble-null geometry of ASDEX Upgrade, with increased lower triangularity, δ_L, and decreased upper triangularity, δ_U, made possible by the new divertor on JET.

JT-60U reported [25] improved H-mode pedestal pressure and energy confinement resulting from the reduction of toroidal field ripple (figure 15).

The H-mode plasma performance could be improved in Alcator C-MOD after applying boron coatings on molybdenum

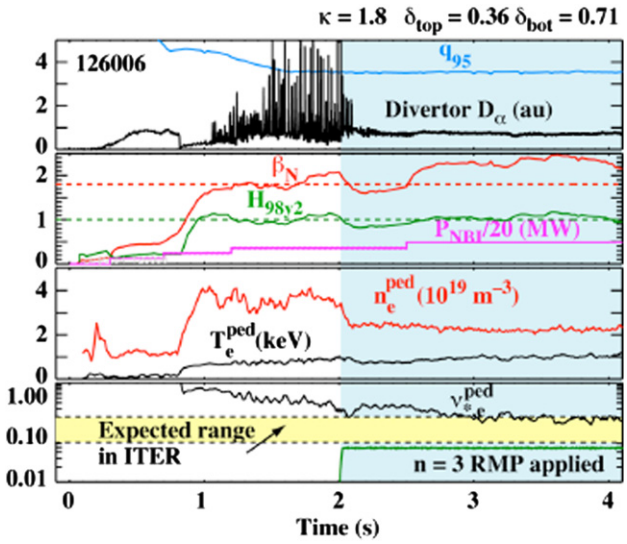

Figure 13. Complete ELM suppression in DIII-D using $n = 3$ RMP in a discharge with a shape and collisionality similar to that in ITER. The dashed lines in the second plot from top represent the ITER $Q = 10$ baseline target values for β_N (red) and $H_{98}(y,2)$ (green).

tiles to reduce the metallic impurity concentration, n_{Mo}/n_e, by a factor of 10–20 and diminish radiative losses, with the confinement enhancement factor H_{89P} over the ITER89-P L-mode power law scaling [36] approaching 2 [37, 38]. A world-record volume averaged plasma pressure ($\langle p \rangle$ = 1.8 atm) at $\beta_N = 1.74$ was subsequently obtained in a boronized discharge.

In TCV, third harmonic X3 ECH (1.5 MW) applied to ELMy H-modes led to $\beta \sim 2.5\%$ ($\beta_N \sim 2$), large type I ELMs and peaked density profiles, significant ion heating (T_i up to ~1 keV, with $T_i/T_e \sim 0.4$), and to a transition to quasistationary ELM-free H-modes (figure 16) lasting for many energy confinement times [39]. This regime on TCV is claimed to have fundamental differences with respect to both the quasistationary ELM-free H-mode observed on DIII-D and the EDA H-mode on ALCATOR C-MOD, based on the fact that it does not have direct ion heating, active fuelling, cryo-pumping, an edge harmonic oscillation and is obtained at $q_{95} \sim 2.5$ (as for instance compared to $q_{95} > 3.7$ on ALCATOR C-MOD).

Improved energy confinement with enhancement factor H_H up to 1.3 has been reported in T-10, following the injection of deuterium pellets, whereby the electron cyclotron power necessary for the transition to improved confinement was found to be 5–10 times lower than the estimated power threshold level from the ITER scaling [40].

4.2.2. The hybrid scenario. Improved performance with respect to the ITER baseline scenario can often be achieved by tailoring the current profile. Scenarios are being developed for ITER with moderate current profile requirements, offering the prospect of improved plasma performance and long pulse inductive operation without a full steady-state capability. These are therefore called 'hybrid scenarios'.

JET and ASDEX Upgrade develop the same type of hybrid scenario, also called improved H-mode, with weak central magnetic shear and central safety factor q_0 above unity.

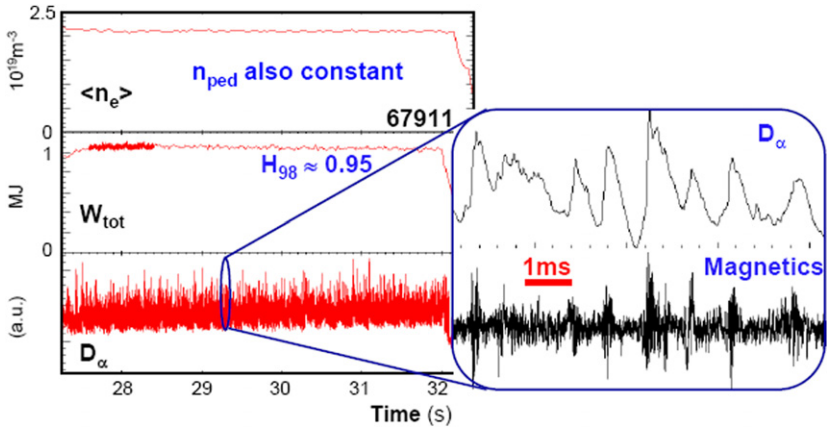

Figure 14. Refined plasma shape has led to stationary benign ELM regime with good confinement in JET. Turbulent magnetic fluctuations coincide with D_α bursts.

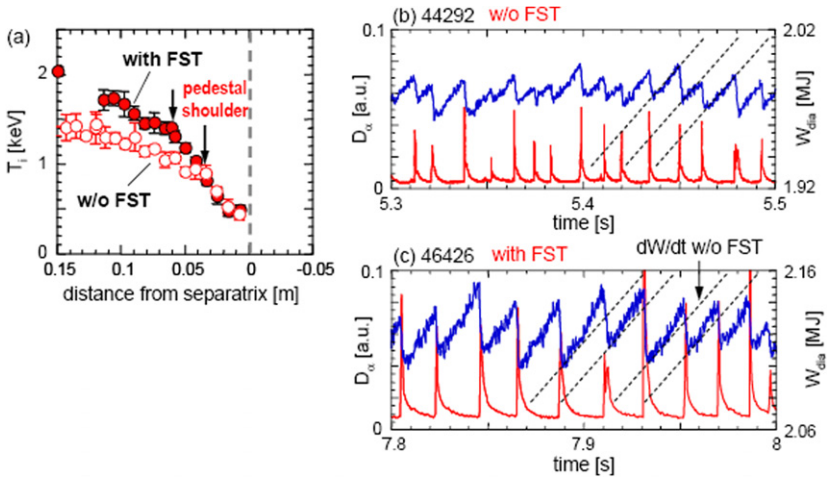

Figure 15. (*a*) T_i profiles in the pedestal region of JT-60U for the cases with and without ferritic steel tiles (FST). The temporal evolution of the D_α emission and W_{dia} for the cases without FSTs (*b*) and with FSTs (*c*). The time derivative of the plasma energy dW/dt during the inter-ELM phase for the case without FSTs is shown as broken lines in (*b*) and (*c*).

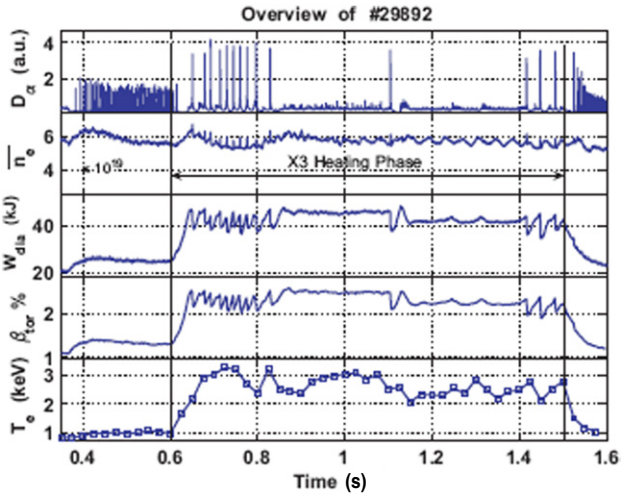

Figure 16. Overview of a TCV discharge (29892) exhibiting a transition to a quasi-stationary ELM-free H-mode. From top to bottom: D_α light, line-averaged density ($n_e \sim$ constant at 7.0×10^{19} m^{-3}, stored energy, β_{tor} and electron temperature. The ELMy H-mode target is heated using ~1.4 MW of X3 ECRH power.

JET experiments [31] show that in this scenario with edge $q_{95} \sim 4$ sawteeth are absent and energy confinement is higher than expected from the IPB98(y, 2) scaling [33], but consistent with the weaker β-dependence found in dedicated confinement scans in JET and DIII-D. The 2006 JET hybrid discharges show improved performance at low $q_{95} \sim 3$ ($\beta_N = 3$), slightly better than the H-mode, with β controlled in real-time (see figure 17). Moreover, the analysis of a newly assembled database of ~100 JET hybrid discharges [41] shows improved core confinement in some cases, with high $T_i(0)$ and $T_e(0)$ up to ~17 keV and 8 keV, respectively, short temperature gradient scale lengths ($R/L_{Ti} > 14$ and $R/L_{Te} > 11$) over a wide region ($\Delta r \sim 0.2$ m) in the plasma core, with a sharp decrease in both ion and electron heat diffusivity χ_i and χ_e over the entire plasma core for more than 5 s.

ASDEX Upgrade has also extended the operational range of the hybrid (or improved H-mode) scenario by optimizing its performance for q_{95} down to 3, on a broad range of ν^* values and at high density, using real-time control of β_N and electron cyclotron current drive (ECCD) to suppress neoclassical tearing modes (NTMs) at low $\beta_N \sim 2$ [42]. Based on these results and on an extrapolation using the ASTRA transport code starting from experimental profiles a favourable

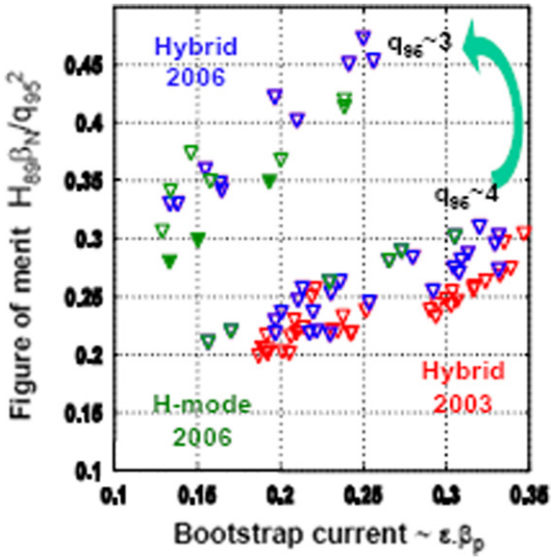

Figure 17. Comparison of performance of recent hybrid and H-mode discharges in JET. At high $q_{95} \sim 4$ the hybrid performance is similar to the H-mode one. At low $q_{95} \sim 3$ the hybrid performance is improved and slightly better than H-mode with β controlled in real time.

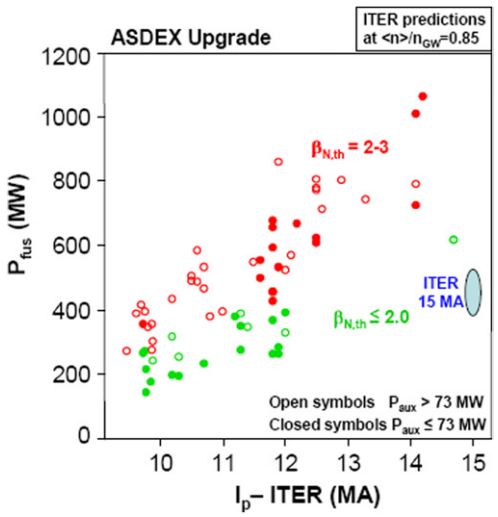

Figure 18. Prediction of the fusion power in ITER by scaling the kinetic profiles data from ASDEX Upgrade. The power requirements (P_{aux}) to sustain the $\beta_{N,th}$ use the IBP98(y, 2) scaling.

prediction of high fusion power ($P_{fus} = 1070$ MW, $Q = \infty$) at $q_{95} = 3.1$ in ITER has been presented (see figure 18). It has to be noted that, by extending the operational range of the hybrid/improved H-mode regime to $q_{95} \sim 3$, JET and ASDEX Upgrade have moved this regime to a domain with a fusion performance G ($= \beta_N H_{89P}/q_{95}^2$) higher than formerly achieved at $q_{95} \sim 4$–5.

Using the new counter-NBI capability [32] to reduce the central Mach number by up to a factor of 6 compared with co-NBI discharges, DIII-D could demonstrate that for hybrid scenarios, although energy confinement decreases and the 3/2 NTM amplitude increases for low Mach number, the fusion performance parameter G still exceeds the value required on ITER for $Q = 10$ ($G = 0.42$). $G = 0.7$ could be maintained

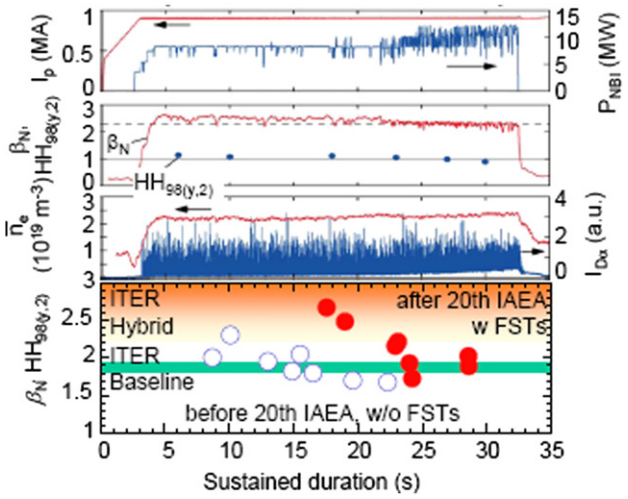

Figure 19. Waveforms of a typical high β_N long pulse plasma in JT-60U. From top to bottom: plasma current and heating power, β_N, and confinement enhancement factor, $H_{H98(y,2)}$, line-averaged density and divertor D_α intensity. Bottom last: Sustained duration of $\beta_N \cdot H_{H98(y,2)}$.

at $q_{95} \sim 3.2$ with stationary conditions for over five current relaxation times [43].

Making use of the installed ferritic steel tiles in JT-60U (see also section 4.1), the duration of high β_N plasmas has been extended close to the hardware limit of heating systems (30 s for the NBI system) [44]. A high confinement plasma ($H_{98}(y, 2) \sim 1.1$, $I_p = 0.9$ MA, $B_T = 1.6$ T, $q_{95} \sim 3.3$, $\delta \sim 0.32$ and $\kappa \sim 1.4$) with $\beta_N \geqslant 2.4$ was kept up to $t \sim 22$ s (figure 19) and a bootstrap current fraction of 36–45% was sustained for 23.1 s (~12 current diffusion time, τ_R) which gives $G > 0.2$.

4.2.3. Advanced tokamak scenarios with ITB. Advanced tokamak scenarios are developed in view of meeting ITER steady-state operation requirements. These scenarios with reversed magnetic shear and ITBs are demanding in terms of current profile control. These are studied and developed in a variety of conditions and current drive schemes on the tokamaks JET, DIII-D, TCV [45], T-10 [46], FTU [47] and JT-60U [44].

In TCV and T-10 electron ITBs are formed using strong ECRH. In the TCV case the confinement improvement over the L-mode ranges from 3 to 6; the bootstrap current fraction is invariably large and is above 70% in the highest confinement cases, with good current profile alignment permitting the attainment of steady state.

In DIII-D the current profile is broadened by a combination of ECCD and a toroidal magnetic field ramp for improved coupling with the wall and active control coils, and $\beta_N \sim 4 \sim 6\, l_i$ (internal inductance) has been maintained for 2 s with ITBs, well above the no-wall stability limit [48]. Recent progress on DIII-D is summarized in figure 20 where the fusion ignition figure of merit G is plotted versus the bootstrap current fraction.

Whereas previous advanced tokamak discharges on JET were studied mainly in a configuration with a low triangularity of $\delta \sim 0.3$, recent advanced tokamak discharges with ITBs have been studied in conditions closer to ITER (see figure 21),

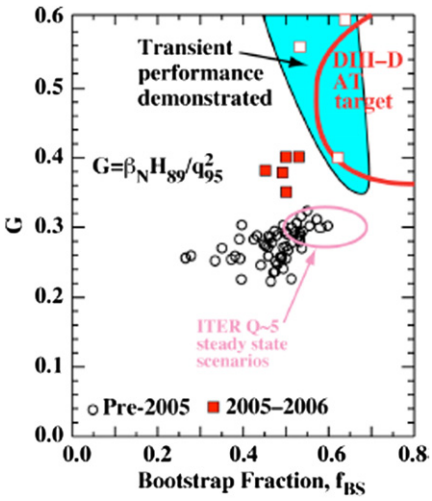

Figure 20. Achieved values of G and bootstrap fraction f_{BS} in DIII-D discharges. The open squares in the shaded region represent discharges using B_T and I_P ramps to transiently achieve high performance while the closed squares use techniques that are in principle capable of steady-state operation. The open circles are from data prior to the 2005 experimental campaign.

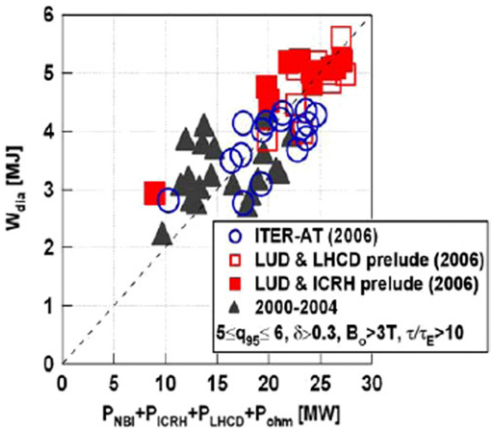

Figure 21. Progress in increasing performance in JET advanced tokamak discharges, including recent results following power upgrades and the installation of a new divertor for high-triangularity operation.

in two new configurations (LUD and ITER-AT). The LUD configuration has a low upper triangularity, $\delta_U \sim 0.2$, but a high lower triangularity, $\delta_L \sim 0.55$, and the ITER-AT configuration has high upper and lower triangularities of $\delta_U \sim 0.45$ and $\delta_L \sim 0.55$ [31, 49]. The LUD configuration was studied with high heating power (27 MW, comprising 20 MW of NB, 5 MW of ion cyclotron resonance heating (ICRH) and 2 MW of lower hybrid current drive (LHCD)) and an ITER-relevant $q_{95} \sim 5$ at 1.9 MA/3.1 T, compared with $q_{95} \sim 7.5$ previously at low $\delta \sim 0.3$. Under these conditions, ITBs were established with simultaneously higher pedestal and core densities ($n_{eped} \sim 2.5 \times 10^{19}\,m^{-3}$ and $n_{e0} \sim 6 \times 10^{19}\,m^{-3}$), with $T_{i0} \sim 8$–10 keV close to $T_{eo} \sim 7$–8 keV (see figure 22) and with ELMs which do not affect the ITB. At peak performance the non-inductive current fraction reached 70%.

In FTU, ECCD and LHCD are used to form and sustain steadily ITBs all along the heating pulse ($>35\,\tau_E$ with τ_E exceeding the ITER97 L-mode confinement scaling [50] by about 1.6 times, $T_{e0} \geqslant 5$ keV) at ITER relevant plasma density ($\geqslant 10^{20}\,m^{-3}$, $n_{e0}/n_{GW} \geqslant 0.9$, n_{GW}: Greenwald density), major advances consisting of the development of methods to control the barrier radial width by adjusting the LHCD deposition profile, with steady ITB radii obtained up to $r_{ITB}/a \geqslant 0.67$.

4.3. Long pulse operation, steady-state and real-time control

The qualification to reactor relevance of plasma confinement experiments includes the demonstration of plasma sustainment much longer than the four characteristic times in fusion plasmas: the energy confinement time (τ_E), the effective particle confinement time (τ_P^*), the current diffusion time (τ_R) and the wall saturation time (τ_W).

Taking advantage of its intrinsic capability of steady-state net-current free plasmas, long pulse operation in the LHD stellarator is primarily sustained by ICRF heating, enabling the creation of high-temperature plasmas maintained for more than 30 min, with a world-record injected heating energy of 1.3 GJ (average heating power of 680 kW, T_{e0} and T_{i0} of 2 keV at $n_e \sim 0.8 \times 10^{-19}\,m^{-3}$) in 2005 and recently for 54 min with 1.6 GJ (average heating power of 380 kW, T_{e0} and T_{i0} of 1 keV at $n_e \sim 0.4 \times 10^{-19}\,m^{-3}$) in the 2006 experimental campaign (see figure 23) [51, 52]. A key player for the reported success was the modification of the three-dimensional heat-deposition profile of the LHD helical divertor in order to effectively disperse the heat load during long pulse discharges using a magnetic-axis swing technique.

The necessity to sustain the current in confinement devices based on net toroidal current such as tokamaks represents a primary limitation in view of long pulse (continuous) and steady-state operation. To prepare for the next generation of steady-state superconducting tokamak experiments such as ITER several present experiments (Tore Supra [53], TRIAM-1M [54], HT-7 [55, 56], DIII-D [32, 48], JET [49, 57], NSTX [58], JT-60U [23]) are therefore addressing key technologies and the physics of non-inductive current drive scenarios, particle control, actively cooled plasma facing components, diagnostics and real-time plasma control using various sets of control tools.

DIII-D being equipped with a set of control tools to allow precise control of key aspects of plasma stability, transport, and current drive, its approach to steady-state operation is to maximize fusion power and bootstrap current (bootstrap current fraction $f_{BS} = 50$–75%) by operating at high normalized beta $\beta_N \geqslant 3.5$ and safety factor $q_{min} > 1.5$, and provide the remaining current with NB (NBCD), ECCD and fast wave (FW) current drive. In this approach two scenarios have been investigated [48], one exhibiting high fusion performance, $G \leqslant 0.7$, but not stationary and another reaching fully non-inductive conditions (non-inductive current fraction $f_{NI} \sim 100\%$) at $G \sim 0.3$ for several confinement times (or about $\tau_R/2$), as foreseen in the ITER $Q = 5$ steady-state scenario.

In HT-7 long pulse discharges at the level of $I_p \sim 60$ kA, $n_{e0} \sim (0.8$–$1) \times 10^{19}\,m^{-3}$ could be extended to times longer than 6 min using about 150 kW of LHCD only [55]. Moreover, a steady-state alternating current (AC) operation mode has been demonstrated up to 53 s in ohmic plasmas and 30 s in

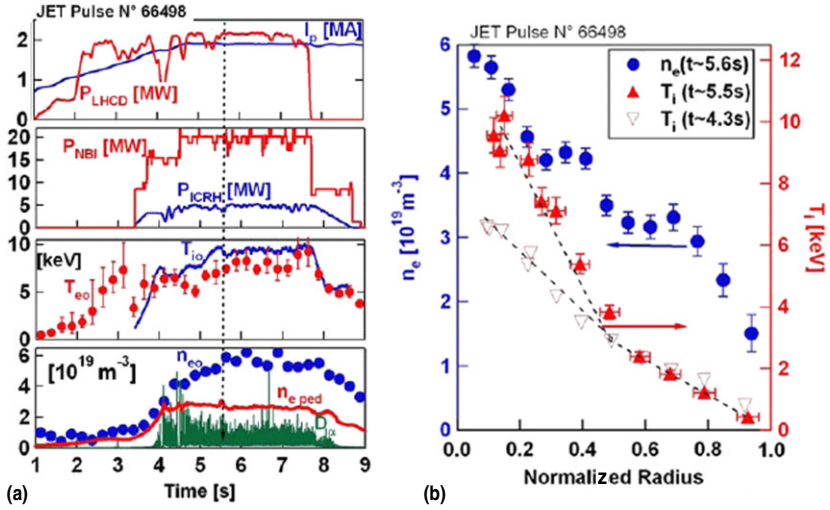

Figure 22. JET: (*a*) time traces of an advanced tokamak discharge in the LUD configuration and (*b*) density and temperature profiles close to the time of peak neutron rate (closed symbols) and, as a reference, the temperature profile prior to ITB formation (open symbols).

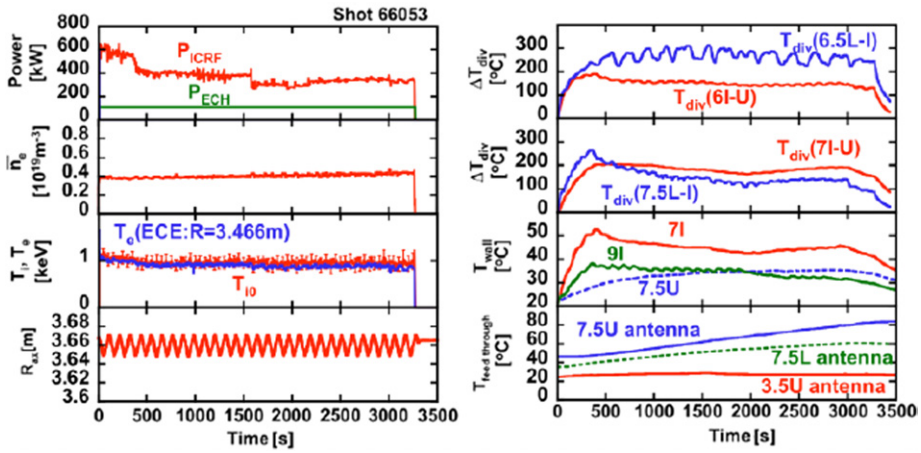

Figure 23. Waveforms of a 54 min long discharge in the LHD stellarator.

LHCD plasmas at the level of $I_p = 100$–125 kA, $n_{e0} \sim (1.5$–$2.5) \times 10^{19}$ m^{-3} [56].

It is essential to demonstrate that active current profile control is compatible with actively cooled plasma facing components protections for durations much longer than τ_R and close to the thermal equilibrium time of plasma facing components. In this regard, making use of a large number of new real-time sensors, Tore Supra has used experimental power flux analyses on the seven infra-red cameras monitoring its five antennas and the toroidal pumped limiter for setting up power load limit avoidance schemes, and successfully combined it with LHCD deposition profile and loop voltage (see figure 24).

Using the motional Stark effect to measure the off-axis current drive, JT-60U has developed a real-time control system of the minimum safety factor q_{min}, which was then subsequently raised, leading to the suppression of MHD fluctuations with the stored energy increased by 16% [59].

Modified plasma control capabilities and poloidal field coils of NSTX have enabled plasmas with high shape factor being sustained for pulse lengths of $1.6\,\text{s} \sim 50\tau_E \sim 5\tau_R$. Also, plasmas with higher $\beta_t = 2\,\mu_0\langle p\rangle/B_T^2 \sim 20\%$ could be sustained for pulse lengths of $1.2\,\text{s} \sim 25\tau_E \sim 3\tau_R$ with non-inductive current fractions $f_{NI} \sim 50\%$ (~40% pressure driven current and ~10% NB driven current) [58].

In JET, real-time simultaneous control of several radially distributed magnetic and kinetic plasma parameters (such as the safety factor, $q(x)$, and gyro-normalized temperature gradient, $\rho^*_{Te}(x)$, respectively) is being investigated in view of developing integrated control of advanced tokamak scenarios and ITBs suitable for ITER [57]. The new model-based optimal profile controller being currently experimentally tested aims at using the combination of heating and current drive systems—and optionally the poloidal field system—in an optimal way to regulate the evolution of several parameters.

4.4. Progress on plasma scenarios in reversed field pinches and helical devices

New high current improved-confinement plasmas have been produced in the reversed field pinch (RFP) experiment MST by applying inductive edge current drive to 500 kA RFP discharges [60]. This edge current replaces fluctuation-driven current, thus leading to more stable plasmas. Magnetic fluctuations are reduced, energy confinement is increased

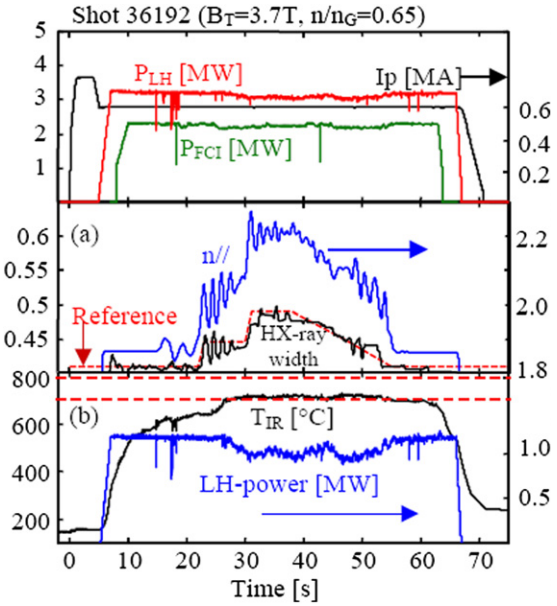

Figure 24. Combined control of the lower hybrid power deposition profile (*a*) with infra-red limit avoidance of plasma facing components on Tore Supra. In (*b*) the infra-red avoidance scheme acts on one of the LH launchers as the temperature reaches its limit of 700°.

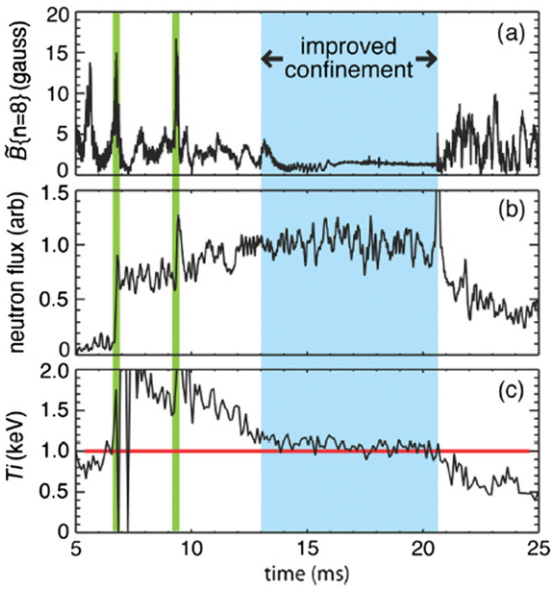

Figure 25. (*a*) Magnetic fluctuation amplitude, (*b*) D–D neutron emission and (*c*) C^{+6} impurity ion temperature during an improved confinement plasma in MST. The two vertical shadings at 7 and 9 ms mark reconnection events during which ions are strongly heated.

ten-fold ($\tau_E \sim 10$ ms), and magnetic relaxation phenomena are strongly reduced (see figure 25).

In the LHD stellarator a new regime of improved confinement with super dense core plasma has been observed in local island divertor discharges [61]. The super dense core plasma has been established naturally by multiple pellet injection and operates at high density ($n(0) \sim 5 \times 10^{20}\,\mathrm{m}^{-3}$, see figure 26). A temperature of 0.85 keV is maintained by an internal diffusion barrier.

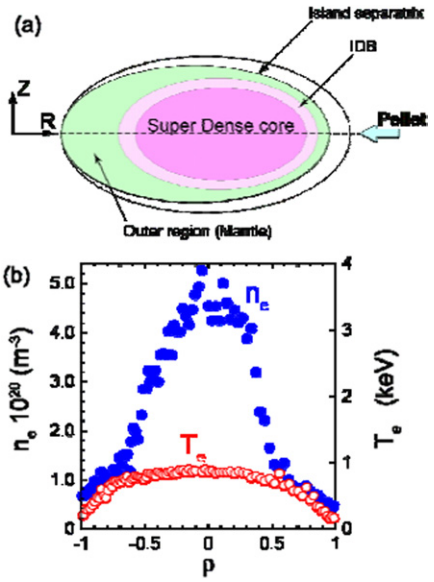

Figure 26. (*a*) Illustration of a super dense core plasma in LHD. (*b*) Density and temperature profiles of a super dense core discharge with $R_{ax} = 3.75$ m, $P = 10$ MW.

The CHS stellarator reported the successful achievement of an H-mode with a high plasma density ($1 \times 10^{20}\,\mathrm{m}^{-3}$) and a high magnetic field, which has been developed with the reheat mode operation technique (figure 27) [62].

4.5. New results on transport and confinement physics

4.5.1. Rotation and confinement, momentum transport. Investigations of the impact of rotation on confinement have been reported from the tokamaks Tore Supra [63], JT-60U [25], JET [31, 64], TCV [65] and DIII-D [43].

In Tore Supra L-Mode discharges with ICRH observation of a spontaneous toroidal counter rotation up to 70 km s^{-1} in the core region, in correlation with confinement improvement (figure 28), has been reported, suggesting the presence of a sheared rotation at $R = 2.8$ m as a candidate to explain stabilization of ion temperature gradient and trapped electron modes (TEMs).

Pedestal parameters and confinement have been shown to be improved with co-rotation following the installation of ferritic steel tiles in JT-60U (see also section 4.1), and fast ion losses due to toroidal field ripple are found to induce toroidal rotation in the direction anti-parallel to the plasma current (counter rotation) [24]. The reduction of the radial electric field attributed to the decrease in the fast ion loss with the ferritic steel tiles is believed to slow down the ctr-rotation at the plasma edge, thus enhancing co-rotation and leading to improved energy confinement [25].

In the MAST spherical tokamak [66] counter-NBI discharges show a factor of ~2 enhancement in confinement over typical co-NBI heated plasmas, resulting in similar levels of plasma performance (even with only ~50% of the NBI power absorbed), with the improvement in confinement appearing to be due to a reduction in transport as a result of increased peripheral $E \times B$ shearing.

While the FT-2 tokamak has demonstrated the possibility of plasma poloidal velocity measurement using the upper

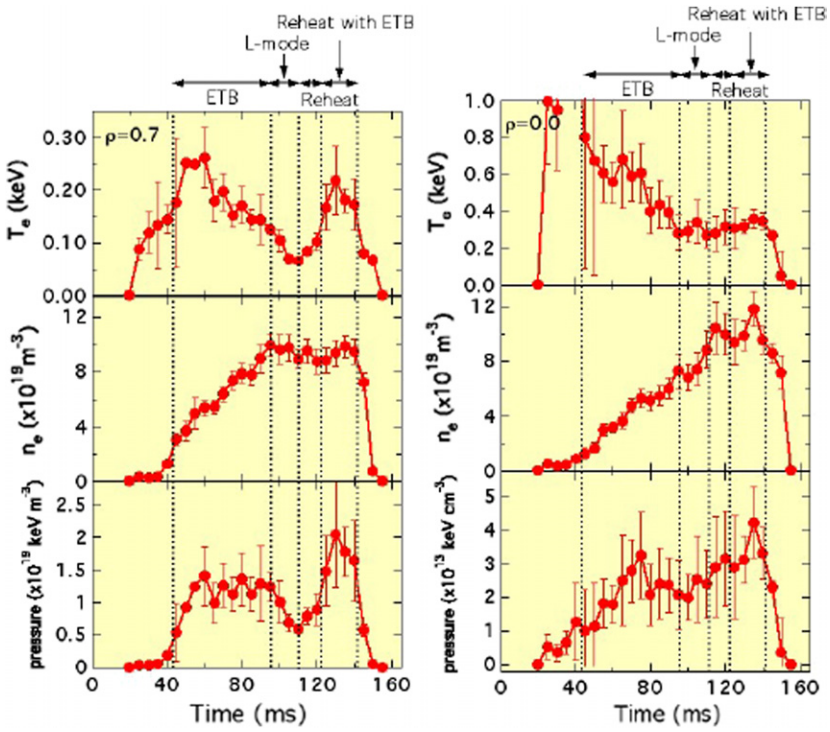

Figure 27. Time behaviour of local electron density and temperature measured by YAG Thomson for edge and central region in a CHS's high density H-mode plasma.

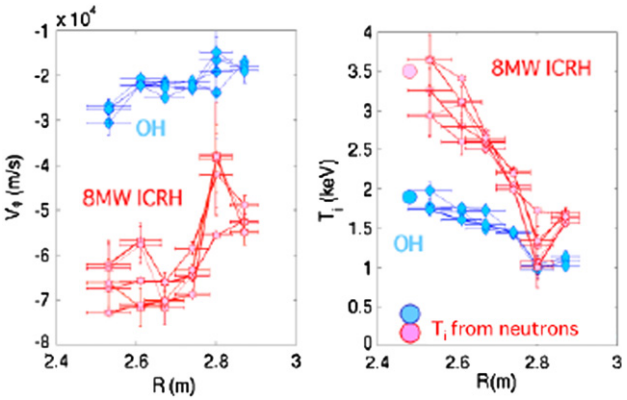

Figure 28. Toroidal rotation velocity (left, measured by CXRS) and ion temperature profile (right) for the ohmic (blue diamond) and ICRH heated (red square) phase of four consecutive high power discharges in Tore Supra. A spontaneous toroidal counter rotation up to 70 km s^{-1} in the core region, in correlation with confinement improvement is observed.

hybrid resonance backscattering signal [67], experimental measurements of poloidal velocities in JET with charge exchange spectroscopy (CXS) show that the carbon poloidal velocity can be an order of magnitude above the neoclassical estimate within an ITB layer [64]. This significantly affects the calculated radial electric field and therefore, the $E \times B$ flow shear used for example in transport simulations. The Weiland transport model well reproduces the onset, location and strength of the ITB when the experimental poloidal rotation is used while it does not predict an ITB when using the neoclassical poloidal velocity. The most plausible explanation for the generation of the anomalous poloidal velocity is proposed to be the turbulence driven flow through the Reynold's stress.

DIII-D profiles with high/low toroidal rotation confirm the importance of $E \times B$ shear for ITBs, and transport physics has been found to be sensitive to applied torque (rotation).

Measurements of the plasma toroidal rotation in the absence of external momentum input in TCV are found to be inconsistent with diffusion of toroidal momentum from the edge region, suggesting instead a change in the balance of internally generated sources of momentum.

Momentum transport studies in JET [64] indicate that the ratio of the global energy confinement time to the momentum confinement is close to $\tau_E/\tau_\phi = 1$ except for low density discharges where the ratio is $\tau_E/\tau_\phi = 2$–3. On the other hand, local transport analysis of tens of discharges shows that the ratio of the local effective momentum diffusivity to the ion heat diffusivity is $\chi_\phi/\chi_I \sim 0.1$–0.4 rather than unity, as expected from the global confinement times and used in ITER predictions. The apparent discrepancy in the global and local momentum versus ion heat transport is explained by the fact that momentum confinement within the edge pedestal is worse than that of the ion heat.

4.5.2. Turbulent transport. The emergence of a multi-faceted picture of mode dominance in different plasma parameter regimes of ion temperature gradient, TEM and electron temperature gradient turbulence has been supported by several toroidal confinement devices including ASDEX Upgrade [30, 68–70] based on detailed measurements including fluctuation reflectometry and gyro-kinetic calculations (see figure 29), T10 [46] based on linear electrostatic calculations, Alcator C-MOD [37] based on non-linear gyro-kinetic

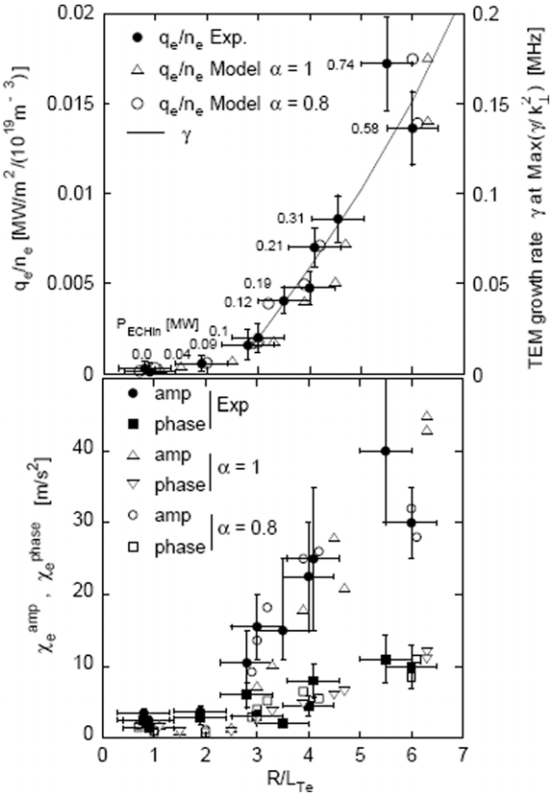

Figure 29. TEM instability threshold in ASDEX Upgrade. Top: electron heat flux versus R/L_{Te}, experimental data, simulations with empirical model and growth rate of the TEM. Bottom: χ_e^{amp} and χ_e^{phase} versus R/L_{Te}, experimental and modelling data.

simulations and comparison with measured density fluctuation spectra, FT-2 [67] based on measurements using a correlative upper hybrid resonance backscattering technique, NSTX [71] based on linear and non-linear simulations combined with measurements using a new high resolution tangential microwave scattering system (280 GHz), MAST [72] based on the combination of high resolution kinetic diagnostics and a suite of turbulence codes and TCV [73] based on measurements and local gyro-fluid and global gyro-kinetic simulations.

The impact of plasma shaping on electron heat transport has been considered in TCV electron cyclotron heated L-mode plasmas with the demonstration of the decrease of the experimental electron heat diffusivity χ_e with decreasing triangularity δ and increasing plasma collisionality ν_{eff} (see figure 30). For higher effective collisionality, ranging from 1 to 2 and achieved in ohmic plasmas, the experimental electron heat transport is no longer observed to decrease with decreasing triangularity.

One of the significant issues found in electron heat transport analysis in the past has been a non-local heat transport phenomenon observed in perturbation experiments on many tokamaks and a few helical systems. In particular, a rise of the core electron temperature T_e invoked by the rapid cooling of the edge plasma has been observed in various tokamaks and the amplitude reversal of the cold pulse propagation in the core plasma could not be explained by a local heat transport model. Extensive parametric studies of non-local T_e rise in LHD [74] have been able to usefully extend the experimental

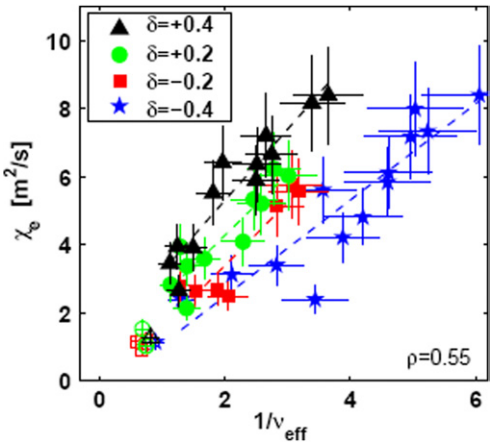

Figure 30. TCV: decrease of the experimental electron heat diffusivity χ_e with decreasing triangularity δ and increasing plasma collisionality ν_{eff} in EC heated L-mode plasmas (full symbols). In high collisionality ohmic plasmas (open symbols) the effect of plasma triangularity on χ_e is no longer observed.

data base to test ion temperature gradient-based transport models which have been proposed to explain the anomalous transport behaviour.

4.5.3. Edge transport barrier studies. Studies related to edge transport barrier formation and performance have been presented from Alcator C-Mod, ASDEX Upgrade, TJ-II [75], LHD [76] and CHX. Highlights include the experimental observation of the correlation between the radial electric field, E_r, and the edge transport barrier formation and strength in ASDEX Upgrade [68], based on measurements using Doppler reflectometry, and in the CHS stellarator [62], based on measurements using CXS. In the plasma edge in ASDEX Upgrade the E_r radial profile shows the narrow negative well coinciding with the steep pedestal pressure gradient whose depth scales with the plasma confinement: from typically $-5\,\mathrm{kV\,m^{-1}}$ in ohmic and L-mode conditions to $-30\,\mathrm{kV\,m^{-1}}$ in H-modes (figure 31), to over $-50\,\mathrm{kV\,m^{-1}}$ in improved H-modes. Furthermore, experiments in Alcator C-Mod [77] suggest a strong role for critical gradient behaviour in setting profile characteristics of edge plasma, in contrast to the frequently used diffusive model for plasma transport modelling.

4.5.4. ITB studies. Transport barrier are regions with low levels of turbulence and heat diffusivity and therefore high-temperature gradients. To different extents, ITB-related studies have been conducted on many devices including JET [31], NSTX [71], CHX [62], T-10 [78], JT-60U [44, 78, 79], FTU [47], TJ-II [80], DIII-D [81], TCV [45], Alcator C-Mod [37] and LHD [82], whose highlights are presented in the following.

According to transport analysis supported by the measured ion temperature profiles, the ion heat conductivity χ_i in FTU's L-mode plasmas with electron ITBs has been found to drop below the neoclassical value inside both narrow and wide ITBs, reaching the ohmic neoclassical level. This is shown in figure 32 where ion heat conductivity profiles are plotted for two different discharges as obtained from

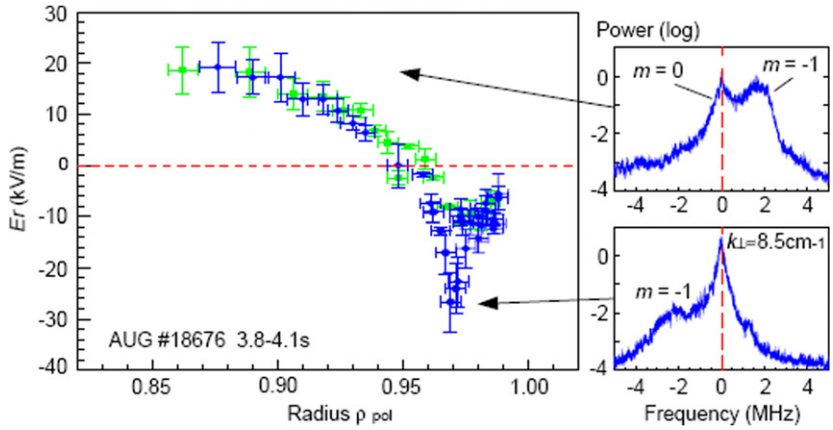

Figure 31. Typical radial electric field E_r profile in ASDEX Upgrade for a -2 T/+1 MA ELMy H-mode (#18676) with 12 MW of NBI heating together with example Doppler spectra showing $m = 0$ and $m = -1$ peaks. The $m = -1$ peak is the Doppler shifted peak which is of most interest for determining E_r. The strength of the E_r well increases directly with confinement, with typically $-5\,\mathrm{kV\,m^{-1}}$ for ohmic and L-mode conditions, jumping to around $-30\,\mathrm{kV\,m^{-1}}$ for H-mode and in excess of $-50\,\mathrm{kV\,m^{-1}}$ for improved H-modes.

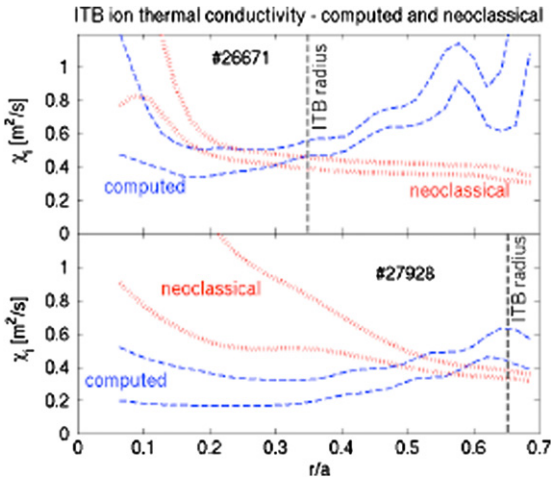

Figure 32. The ion heat conductivity χ_i in FTU's L-mode plasmas with electron ITBs is found to drop below the neoclassical value inside both narrow and wide ITBs, reaching the ohmic neoclassical level. Here, χ_i profiles are plotted for two different discharges as obtained from computations using experimental ion temperature profiles and from neoclassical transport theory calculations. Dotted and dashed lines limit the variability range of χ_i during the whole ITB phase.

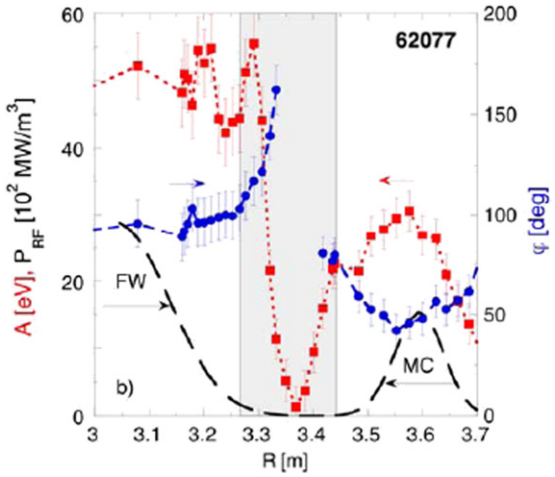

Figure 33. Illustration of a JET discharge in which off-axis T_e modulation was provided by MC of ICRH power, with an additional core modulation due to FW deposition. Two heat waves are then propagating towards the ITB (grey vertical band) from both sides of it. The figure shows that the ITB introduces sharp discontinuities in the slopes of the amplitude (red squares) and the phase (blue dots) of the propagating heat waves, showing the ITB as a narrow layer with reduced heat diffusivity.

computations using experimental ion temperature profiles and from neoclassical transport theory calculations. Moreover, in high density discharges, ion confinement is found to remain good even under important collisional heating and the electron–ion collisions do not prevent the establishment of electron ITBs. However, T_{i0} remains substantially lower than T_{e0} since the electron–ion collision time $\tau_{ei,th} \sim 6\,\tau_E$ (typically 180 against 20 ms).

The propagation of T_e modulations using mode conversion (MC) ICRH both inside and outside an ITB in JET has been used to confirm previous observations of an ITB as a well-localized narrow layer with low heat diffusivity (figure 33), though indicating that ITBs are regions of improved confinement which exhibit a lack of stiffness and sub-critical transport, that is well below threshold [83].

The role of rational safety factor q surfaces in the formation of an ITB has been addressed by most of the above-mentioned devices. In particular, O-mode interferometry measurements on JET reversed magnetic shear plasmas and experimental observations of T_e, T_i, poloidal flow velocity and fluctuation measurements that qualitatively match predictions from GYRO code in DIII-D have commonly led to the observation that the formation of an ITB appears to occur when q_{min} exists and approaches (rather than reaches) an integer value (figures 34 and 35). In both reported cases the ITB formation starts before the $q = 2$ surface enters the plasma. Moreover, a model for core barrier formation based on the GYRO code results that predict profile corrugations in the vicinity of low order rational q surfaces has been developed in DIII-D [81]. It is believed that the profile corrugations are

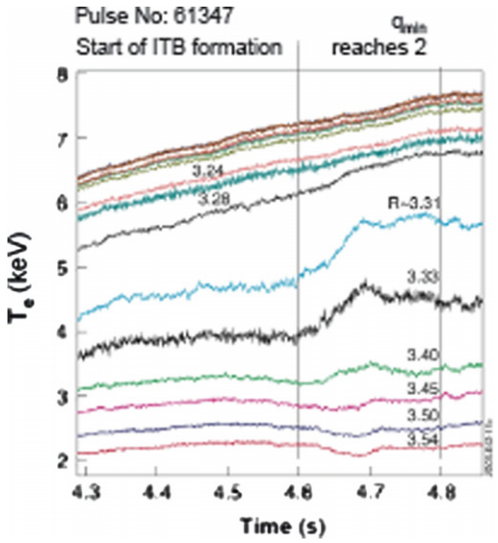

Figure 34. Electron temperature T_e at various major radii, R, showing formation of an ITB in JET.

a manifestation of zonal flow structures that have significant radial extent in the case of large flat shear regions in negative central shear discharges.

As in tokamaks, the TJ-II stellarator observed transitions to improved core electron heat confinement triggered by low order rational surfaces. Transitions triggered by the low order rational surface $m/n = 4/2$ show an increase in the ion temperature synchronized with the increase in the electron temperature (figure 36), which is remarkable since ion temperature changes had not been previously observed either in TJ-II or in any other helical device.

4.5.5. Zonal flows and turbulence. Zonal flows are fluctuations linearly stable but non-linearly driven by turbulence. They are characterized by their symmetric nature around the magnetic axis, that is, $m = n = 0$ (poloidal and toroidal mode number) structure in poloidal and toroidal directions, and have a rapidly varying structure with a finite wavelength in the radial direction. The symmetric characteristics of zonal flows result in the fact that no cross-field transport is associated with them. The investigation of zonal flows and their impact on transport has turned out to be an example of fruitful interaction with other scientific communities and between forward looking theoreticians, 'smaller' devices of all types (tokamaks, helical devices, etc) which are flexible and well diagnosed, and larger devices (sometimes driving specific diagnostics improvements).

At this conference the present worldwide status of experiments on zonal flows was overviewed in [84]. The outcome of this overview includes the fact that the innovative use of traditional and modern diagnostics has revealed unambiguously the existence of zonal flows, their spatio-temporal characteristics, their relationship with turbulence and their effects on confinement. Two kinds of zonal flows have been expected and observed in toroidal plasmas: stationary zonal flows and oscillatory geodesic acoustic modes. In particular, a number of observations have been accumulated on the geodesic acoustic modes [68, 85–88], suggesting the need for theories providing a proper description. Geodesic acoustic modes are found to be localized in a rather narrow region of plasmas with a constant frequency, showing an eigenmode property. The observed geodesic acoustic mode frequencies obey the theoretical expectation. However, the prediction of the selective growth of the eigenmode having an observed frequency is still not yet possible, due to the lack of an appropriate theory. As mentioned in [84], all the experimental observations up to date demonstrate that zonal flows do regulate plasma turbulence and resultant transports. Therefore, this experimental fact supports the theoretical expectation that better confinement is achieved when the ratio of zonal flow to turbulence is larger and indicates a future experimental direction to investigate the issue of: in which conditions can a zonal flow grow along with suppressing turbulence? This answer could be a key to optimizing the magnetic configuration for improved confinement.

4.5.6. Scaling studies. Confinement prediction for the next step machines such as ITER remains challenging for transport models, and still relies on extrapolations of scaling laws based on multi-machine data bases. Indeed, dimensionless analysis provides a natural method for relating confinement experiments to plasma theory, and for extrapolating experimental results to next step machines.

Integrated dimensionless confinement studies performed recently on the tokamaks JET, C-Mod, JT-60U, DIII-D and Tore Supra have been reported [89]. Within these studies, analysis of ELMy H-mode identity experiments on JET and C-Mod shows that, despite results indicating confinement falls as density approaches the Greenwald limit, the Greenwald fraction is not a relevant parameter for confinement scaling, but collisionality (ν^*) is. However the ν^* dependence in the ITER Physics Base ELMy H-mode scaling IPB98$(y, 2)$ [33] seems to be incorrect. Therefore, more experiments are planned to try to resolve the ν^* scaling, including a JET ELMy H-mode ν^* scan.

Studies on JT-60U show a fall in ELMy H-mode confinement with increasing β, contrasting with those on DIII-D and JET which showed a negligible effect. Analysis of a multi-machine database indicates that the differing results may be due to a change in β dependence with plasma shape.

Tore Supra experiments show a negligible β (β exponent ~ -0.2 compared with -1.6 in the ITER L-mode scaling) effect on L-mode confinement [90], suggesting that any β dependence observed in ELMy H-modes is related to the edge pedestal, with a 'two-term' core-pedestal confinement scaling supporting this conclusion.

In other confinement scaling studies [71], it was found that, in contrast to the results obtained in the Mega Ampère Spherical Tokamak (MAST) [72], the IPB98$(y, 2)$ scaling [33] did not adequately describe the NSTX confinement times, and the NSTX dataset submitted to the International Tokamak Physics Activity (ITPA) H-mode database, along with data from the low aspect ratio devices MAST and START (which now significantly extend the range of the inverse aspect ratio $\varepsilon = a/R$ and thermal toroidal β in the ITPA H-mode confinement database) and the standard selection set of higher aspect ratio data [91], were used to develop new scalings [92]. The new scalings showed a stronger scaling with inverse aspect ratio ($\tau_E \sim \varepsilon^{1.03}$ versus $\varepsilon^{0.58}$ as in $98y, 2$) and a

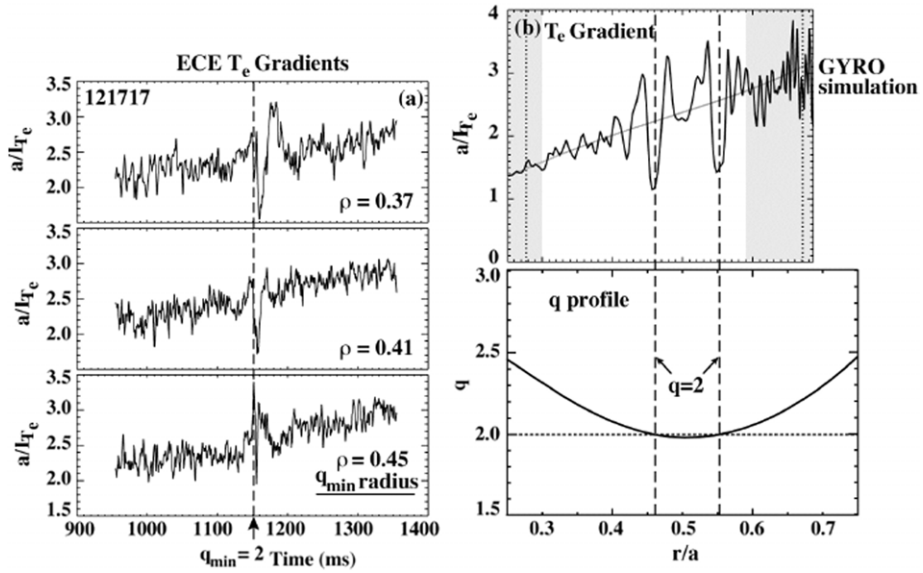

Figure 35. (*a*) $\nabla T_e(t)$ around the $q_{\min} = 2$ time for three locations near the $q_{\min}$ radius for a typical ITB shot in DIII-D, (*b*) T_e gradient versus normalized radius from a GYRO code simulation using the plasma conditions from shot 121717 at 1155 ms and the q profile for this timeslice.

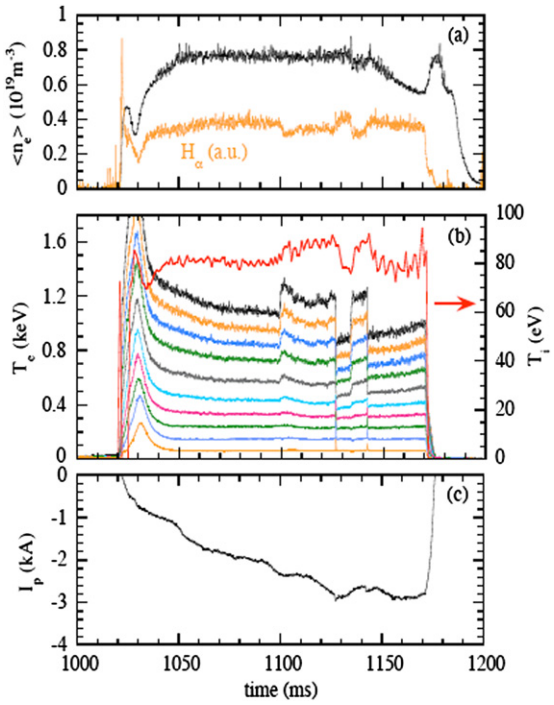

Figure 36. Time evolution of (*a*) line density and H_α signal, (*b*) electron temperature at several radii and ion temperature measured along a central plasma chord and (*c*) net plasma current in TJ-II.

weaker degradation with β_T ($B\tau_E \sim \beta_T^{-0.5}$ versus $\beta_T^{-0.9}$ as in $98y, 2$). It has to be noted that the change in the ε coefficient was accompanied by changes in the I_p, B_T and R coefficients as well. In fact, these studies indicate a strong B_T dependence, with a current dependence that is weaker than that observed at higher aspect ratio ($\tau_E \sim B_T^{0.9} I_P^{0.4}$). The increase of confinement with B_T is claimed to be due to reduced transport in the electron channel, while the improvement with plasma current should be due to reduced transport in the ion channel related to the decrease in neoclassical transport levels. Moreover, dedicated dimensionless parameter scans in NSTX have shown a strong increase of confinement with decreasing collisionality, and only a very weak degradation with β_T, a result which gives good prospects for success of the advanced operating scenario on ITER.

A dedicated plasma current scan ($I_p = 0.6$–1.2 MA) in MAST L-mode plasmas, at constant density, showed that the scaling of energy confinement time with plasma current is similar to that given by by the L-mode scaling ITER97-L [50] (which generally underestimates confinement in MAST L-mode plasmas [93]), $\tau_E \sim I_P^{0.96}$ [72]. Furthermore, co-ordinated studies on MAST and DIII-D demonstrate a strong link between the aspect ratio and beta scaling of H-mode energy confinement, consistent with that obtained when MAST data were merged with a subset of the ITPA database.

In LHD discharges with local island divertor configuration [51], the energy confinement time was found to be improved with respect to the International Stellarator Scaling ISS95 [94] as shown in figure 37, and the state of good confinement could be extended to extremely high density regimes thanks to the formation of an internal diffusion barrier.

The physical model assessment of the energy confinement time scaling in stellarators by making use of the International Stellarator Confinement Database (ISCDB) has been reported to be an ongoing effort [95], with future plans including the extension of the global 0D data base towards profile documentation of existing helical devices.

Finally, with the goal of revealing the underlying mechanism(s) and extrapolating to future devices, paper [96] presented a study of combined parametric scalings of the intrinsic (spontaneous, with no external momentum input) toroidal rotation as observed on a large number of tokamaks. Important conclusions include the following: (i) the intrinsic rotation velocity has been found to increase with plasma stored energy or pressure in JET, Alcator C-Mod, Tore Supra, DIII-D, JT-60U and TCV, and to decrease with increasing plasma

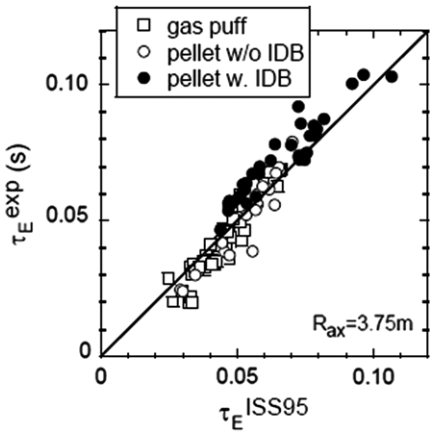

Figure 37. Comparison of the energy confinement time in the local island divertor experiments in LHD with the prediction from the ISS95 scaling.

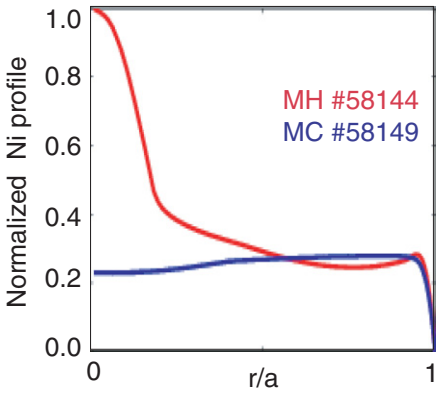

Figure 38. Comparison of Ni transport in ELMy H-modes with ICRH ^{3}He MC heating and MH in JET. The picture shows steady-state profiles of Ni density as obtained from an extrapolation of determined transport coefficients.

current in some of these cases, (ii) the scaling M_A (Alfven Mach number) $= \beta_N/40\pi$ is suggestive of an underlying MHD mechanism, although perhaps not a direct effect, (iii) scalings of the intrinsic rotation velocity with normalized gyro-radius or collisionality show no correlation, (iv) for an ITER discharge with $\beta_N = 2.6$, an intrinsic rotation with Alfven Mach number of $M_A \sim 0.02$ may be expected from the above scaling, possibly high enough to stabilize resistive wall modes without external momentum input.

4.5.7. Particle transport and peaking of the density profile. Peaking of electron and fuel density profiles would be beneficial in fusion reactor plasmas by providing the advantage of higher reactivity, higher bootstrap fraction and stronger electron–ion coupling in the core, than obtained with flat density profiles at the same average density and stored energy. On the other hand, if the profile peaking of impurities becomes stronger than that of the main ions, i.e. if impurities accumulate, excessive fuel dilution occurs. An ITER plasma scenario has to guarantee tolerable radiated power, a particular concern for highly charged impurities with a high associated cooling factor. Tungsten concentration cannot exceed 10^{-4} in the core for stable plasma operation in ITER [28].

According to the present understanding, the main cause for density peaking appears to be an anomalous pinch (and not the Ware pinch or the particle source) as obtained from studies on the tokamaks JET, ASDEX Upgrade and TCV [97]. However, state-of-the art agreement of some gyro-kinetic theory predictions and experimental observations has not yet been demonstrated. Results presented in [97] from an extensive database analysis of JET and ASDEX Upgrade density profiles in H-mode show that the density peaking factor $n_{e0}/\langle n_e \rangle$ increases to above 1.5 as the effective collisionality drops to values close to those expected for ITER. It is claimed that the most important parameters for peaking are collisionality, the beam source (where applicable) and the Greenwald fraction. Scaling expressions including collisionality predict fairly peaked density profiles for ITER ($n_{e0}/\langle n_e \rangle \sim 1.4$), providing a fusion power increase of nearly 30%. However, for this prediction of power increase to be on a solid basis, a full assessment of the impact of predicted density profile peaking on impurity is required.

In TCV L-mode discharges, density peaking is reported [98] to depend mainly on current profiles whereas, in the regions of strong electron transport barrier, density profiles are coupled with electron temperature profiles. The dominant edge safety factor dependence in L-mode is supportive of turbulent equipartition theory, which predicts inward convection in the presence of turbulence whereas the correlation of the density peaking with temperature gradients in electron ITB regimes points to the dominance of the turbulence of the thermo-diffusive type.

JET [99] and ASDEX Upgrade [30] have demonstrated that core impurity peaking in ELMy H-mode plasmas can be controlled with central electron heating. In JET, a pinch reversal for nickel (Ni) impurity is observed when switching from ICRF minority heating (MH) to MC heating (figure 38). This pinch reversal could be explained qualitatively within the framework of ion temperature gradient and TEM instabilities, by a transition in the dominant instability driving Ni transport and in particular to a pinch mechanism connected with the parallel dynamics of the impurities. The measured peaking factor at mid-radius is mentioned to be closer in value to turbulent transport theory predictions than neoclassical theory. The anomalous peaking factor is positive and independent of the charge for neon, argon and Ni as predicted by the linear gyro-kinetic calculation, whereas carbon is negative in contrast to the prediction.

4.5.8. Specific stellarator studies. The first operational quasisymmetric stellarator HSX reported a comparison between the quasihelically symmetric (QHS) configuration and a configuration with the symmetry intentionally broken [100]. The effects of the quasisymmetry have been observed to affect both particle and electron heat transport. Due to the reduced neoclassical thermodiffusion, QHS plasmas have centrally peaked density profiles, in contrast to the hollow profiles observed when the symmetry is broken. Additionally, higher electron temperatures are achieved in QHS plasmas for a fixed input power (figure 39). Experiments with matched temperature profiles indicate that the heat transport in QHS

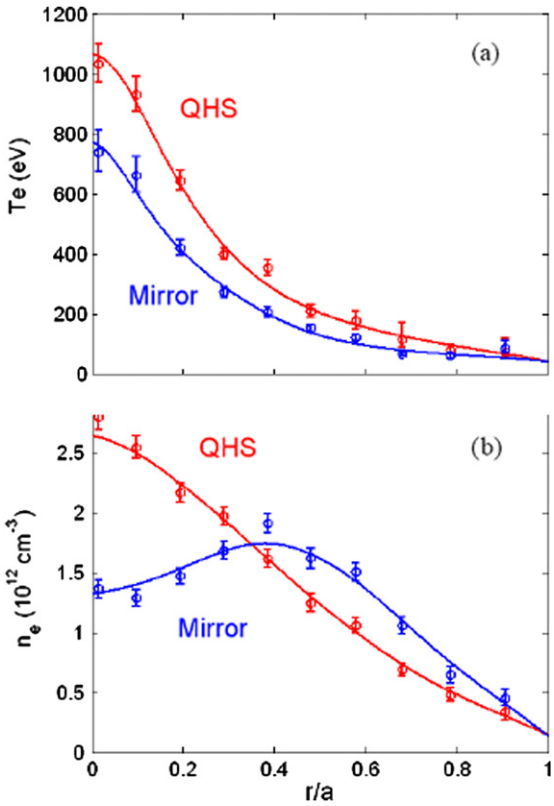

Figure 39. HSX stellarator: profiles of (*a*) electron temperature and (*b*) density in QHS and mirror plasmas. These plasmas are heated with 80 kW of ECRH.

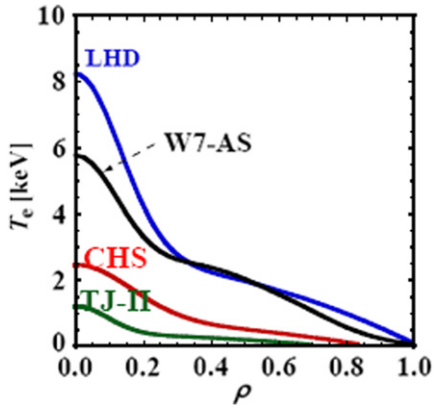

Figure 40. T_e profiles, for example, core electron-root confinement discharges in four stellarator devices.

plasmas is lower than in mirror configurations by an amount consistent with the neoclassical predictions. These results demonstrate that reducing neoclassical transport through quasisymmetry leads to reduced experimental transport. An unexpected consequence of the improved confinement in the QHS configuration is that an Alfvénic instability driven by fast electrons is experimentally observed for the first time. The mode is coherent and global, peaking in the plasma core, and has characteristics consistent with global Alfvén eigenmodes. When symmetry is broken, the mode is no longer observed.

Similarity studies in the helical devices CHS, LHD, TJ-II and W7-AS, reported in [101], have led to the common finding

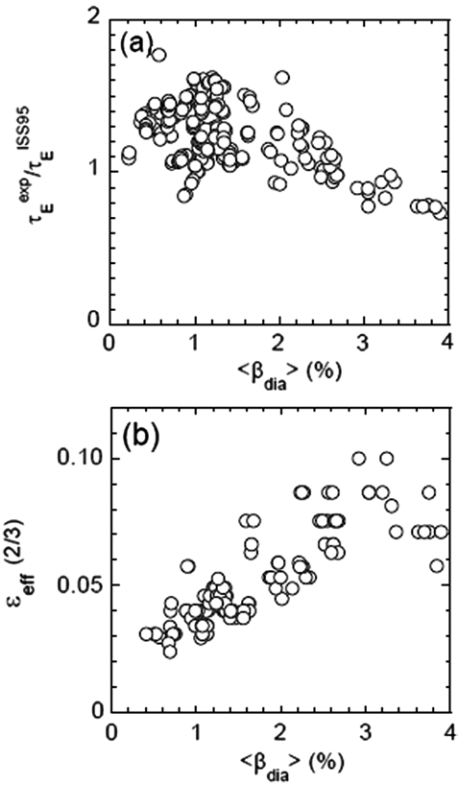

Figure 41. LHD: enhancement factor of the energy confinement time over the ISS95 scaling and the effective helical ripples at $\rho = 2/3$ as a function of beta in the configuration with $R_{ax} = 3.6$ m, $A_p = 6.3$.

of a core electron-root confinement, as shown in figure 40. It is claimed that the core electron-root confinement is based on a different mechanism than the ITB in tokamaks and is clearly identified as an improved electron energy confinement related to the transition to the electron-root solution of the ambipolarity condition, as predicted by neoclassical transport theory in low-collisional helical plasmas.

Observations of the effect of the effective ripple on confinement have been reported in Heliotron J [102] and LHD [51], suggesting that lower effective ripple configurations provide better thermal confinement. In LHD's high-β regime the degradation of confinement (see figure 41) is attributed to global dependence of effective helical ripple on neoclassical transport and not on the MHD effect.

5. Summary and conclusions

Significant advances, with respect to the 20th IAEA Energy Conference, reported at this conference cover the following areas:

Plasma scenarios

Stellarators

- In LHD, an internal diffusion barrier achieved by a combination of efficient pumping of the local island divertor function and core fuelling by pellet injection has enabled a super dense core plasma with n_{e0} as high as 5×10^{20} m^{-3}.

Tokamaks: ITER-relevant scenarios

- Operation at more ITER-relevant parameters (rotation, ν^*, T_e/T_i, n/n_G).
- Real-time control expanding and getting more integrated.
- ELMy H-mode: some progress towards active control of ELMs or moderate ELMs regimes.
- Progress on ITB regimes with $G = \beta_N H_{89P}/q_{95}^2$ above the ITER target, in steady state with dominant bootstrap current.
- Rapid developments on hybrid regimes with extension of operational space up to lower $q_{95} \sim 3$ (i.e. towards improved fusion performance).

Physics (transport and confinement)

- Significant peaking of the density profile predicted for ITER from an empirical approach. However, the issue of density peaking remains a puzzle to theory and modelling.
- A weak (inverse) dependence of global energy confinement and local transport on β, which would be very favourable for ITER, needs to be consolidated.
- The importance of rotation and rotation shear was confirmed and growing interest towards more ITER-relevant rotation patterns is emerging.
- Extensive studies of turbulence and mode dominance in different plasma parameter regimes of ion temperature gradient, TEM and electron temperature gradient.
- Dramatic progress on physics of zonal flows and their interplay with turbulence.
- The role of rational surfaces on the formation of ITBs could be linked to zonal flows.

References

Most of the papers listed below have been presented at the Conference and can be found at http://www-naweb.iaea.org/napc/physics/FEC/FEC2006/html/index.htm

[1] Kotschenreuther M. *et al* On heat loading, divertors and reactors Paper IC/P7-12
[2] Campbell D.J. 2001 *Phys. Plasmas* **8** 2041–9
[3] Kulygin V.M *et al* Project EPSILON—the way to steady state high β fusion reactor Paper IC/P7-1
[4] Kadomtsev B.B. 1960 Magnetic traps with rippled magnetic field *Plasma Physics and the Problem Of Controlled Thermonuclear Reactions* vol 3 ed M.A. Leontovich (New York: Pergamon)
[5] Yoshida Z. and Mahajan S.M. 2002 Variational principles and self-organization in two-fluid plasmas *Phys. Rev. Lett.* **88** 095001
[6] Yoshida Z. *et al* Magnetosphere-like plasma produced by ring trap 1 (RT-1)—a new approach to high-beta confinement Paper IC/P7-14
[7] Kesner J. *et al* First experiments to test plasma confinement by a magnetic dipole Paper IC/P7-7
[8] Jarboe T.R. 1999 *Fusion Technol.* **36** 85
[9] Jarboe T.R. *et al* Spheromak formation by steady inductive helicity injection Paper IC/P7-6
[10] Gerhardt S.P. *et al* Studies of free-boundary field-reversed configurations with improved stability in the magnetic reconnection experiment Paper IC/P7-13
[11] Guo H.Y. *et al* Improved stability and confinement in a self-organized high-β spherical-torus-like field-reversed configuration Paper IC/P7-10
[12] Astrelin V.T. *et al* 1998 Generation of ion-acoustic waves and suppression of heat transport during plasma heating by an electron beam *Plasma Phys. Rep.* **24** 414
[13] England A.C. *et al* Mirror stabilization experiments in the Hanbit mirror device Paper IC/P7-17
[14] Ivanov A.A. *et al* 1994 Experimental study of curvature driven flute instability in the gas-dynamic trap *Phys. Plasmas* **1** 1529
[15] Beklemishev A.D. 2007 Bounce instability in a multi mirror trap *Trans. Fusion Sci. Technol.* **51** 180–2
[16] Burdakov A.V. *et al* Studies of plasma confinement lin GOL-3 multi mirror trap Paper EX/P7-8
[17] Kruglyakov E.P. *et al* Modern mirror systems. Status and perspectives Paper EX/P7-9
[18] Cho T. *et al* Progress in potential formation and radial-transport-barrier production for turbulence suppression and improved confinement in GAMMA 10 Paper EX/P7-14
[19] Cho T. *et al* 2006 *Phys. Rev. Lett.* **97** 055001
[20] Cho T. *et al* 2005 *Phys. Rev. Lett.* **94** 085002
[21] Wan Y *et al* Overview progress and future plan of EAST project Paper OV/1-1
[22] Shinohara K. *et al* Ferritic insertion for reduction of toroidal magnetic field ripple on JT-60U Paper FT/P5-32
[23] Takenaga H. *et al* Overview of JT-60U results for development of steady-state advanced tokamak scenario Paper OV/1-2
[24] Yoshida M. *et al* Driving mechanism of toroidal rotation and momentum transport in JT-60U Paper EX/P3-22
[25] Urano H. *et al* Enhanced H-mode pedestal and energy confinement by reduction of toroidal field ripple in JT-60U Paper EX/5-1
[26] Janeschitz G. *et al* 2001 *J. Nucl. Mater.* **1** 290
[27] Bolt H. *et al* 2002 *J. Nucl. Mater.* **43** 119
[28] Neu R. *et al* 2005 *Nucl. Fusion* **45** 209
[29] Dux R. *et al* Tungsten as first wall material in ASDEX Upgrade Paper EX/3-3Ra
[30] Gruber O. Overview of ASDEX Upgrade results Paper OV/2-2
[31] Watkins M.L. Overview of JET results Paper OV/1-3
[32] Wade M.R. Development in the DIII-D tokamak of advanced operating scenarios and associated control techniques for ITER Paper OV/1-4
[33] ITER Physics Basis 1999 *Nucl. Fusion* **39** 2137
[34] Evans T.E. *et al* 2004 *Phys. Rev. Lett.* **92** 235003
[35] Evans T.E. *et al* 2006 *Nature Phys.* **2** 419
[36] Yushmanov P.N. *et al* 1990 *Nucl. Fusion* **30** 1999
[37] Scott S. *et al* Overview of Alcator C-MOD research program Paper OV/3-2
[38] Marmar E. *et al* Operation of Alcator C-MOD with high-Z plasma facing components with and without boronization Paper EX/3-4
[39] Porte L. *et al* Plasma dynamics with second and third harmonic ECRH on TCV tokamak Paper EX/P6-20
[40] Pavlov Yu.D. *et al* Transport barriers and H-mode in regimes with deuterium pellets injected into T-10 plasma heated by ECR Paper EX/P3-11
[41] Crisanti F. *et al* JET hybrid scenarios with improved core confinement Paper EX/P1-1
[42] Sips A.C.C. *et al* The performance of improved H-modes at ASDEX Upgrade and projection to ITER Paper EX/1-1
[43] Politzer P.A. *et al* Physics advanced in the ITER hybrid scenario on DIII-D Paper EX/P1-9
[44] Oyama N. *et al* Improved Performance in long-pulse ELMy H-mode plasmas with internal transport barrier in JT-60U Paper EX/1-3
[45] Coda S. *et al* The physics of electron internal transport barrier in the TCV tokamak Paper EX/P1-11
[46] Kislov D.A. Overview of T-10 results Paper OV/4-3
[47] Pericoli Ridolfini V. *et al* Internal transport barriers in FTU at ITER relevant plasma density with pure electron heating and current drive Paper EX/P1-15

[48] Greenfield C.M. *et al* Progress toward high performance steady-state operation in DIII-D Paper EX/1-2
[49] Litaudon X. Prospects for steady-state scenarios on JET Paper EX/P1-12
[50] Kaye S.M. *et al* 1997 *Nucl. Fusion* **37** 1303
[51] Motojima O. *et al* Extended steady-state and high-beta regimes of net-current free heliotron plasmas in the Large Helical Device Paper OV/2-1
[52] Mutoh T. *et al* Steady state operation of ICRF heated plasma in the Large Helical Device Paper EX/P1-14
[53] Joffrin E. *et al* Physics of operational integrated controls for steady state scenario Paper EX/1-6
[54] Sato K.N. *et al* Overview of recent experimental studies on TRIAM-1M Paper OV/P-2
[55] Wan B. *et al* Recent experiments in the HT-7 superconducting tokamak Paper OV/P-1
[56] Li J. *et al* Steady-state AC plasma current operation in HT-7 tokamak Paper EX/P1-6
[57] Moreau D. *et al* New dynamic-model approach for simultaneous control of distributed magnetic and kinetic parameters in the ITER-like JET plasmas Paper EX/P1-2
[58] Gates D.A. *et al* Progress towards steady state at low aspect ratio on the National Spherical Torus Experiment (NSTX) Paper EX/P1-3
[59] Suzuki T. *et al* Off-axis current drive and current profile control in JT-60U Paper EX/6-4
[60] Den Hartog D.J. *et al* Overview of results in the MST reversed-field pinch experiment Paper EX/8-2
[61] Ohyabu N. *et al* Super dense core plasma due to internal diffusion barrier in LHD Paper EX/8-1
[62] Okamura S. *et al* Progress of confinement physics study in compact helical system Paper EX/5-5Rb
[63] Chatelier M. Integration of high power, long pulse operation in Tore Supra in preparation for ITER Paper OV/3-1
[64] Tala T. *et al* Overview of toroidal and poloidal momentum transport studies in JET Paper EX/P3-16
[65] Fasoli A. Overview of TCV results Paper OV/3-3
[66] Akers R.J. *et al* The influence of beam injection geometry upon transport and current drive in the MAST spherical tokamak Paper EX/P3-13
[67] Gusakov E.Z. *et al* Investigation of ETG mode micro turbulence in FT-2 tokamak Paper EX/P4-32
[68] Conway G.D. *et al* Study of turbulence and radial electric field transitions in ASDEX Upgrade using Doppler reflectometry Paper EX/2-1
[69] Angioni C. *et al* Theoretical understanding of core transport phenomena in ASDEX Upgrade Paper EX/8-5Rb
[70] Jenko F. *et al* Microturbulence in magnetic fusion devices: new insights from gyrokinetic simulation and theory Paper EX/8-5Ra
[71] Kaye S.M. *et al* Confinement and transport in the National Spherical Torus Experiment (NSTX) Paper EX/8-6
[72] Lloyd B. *et al* Overview of physics results from MAST Paper OV/2-3
[73] Camenen Y. *et al* Impact of plasma shaping on electron heat transport in TCV L-mode plasmas at various collisionalities Paper EX/P3-20
[74] Tamura N. *et al* Impact of nonlocal electron heat transport on the high temperature plasmas of LHD Paper EX/5-6
[75] Pedrosa M.A. *et al* Transport and fluctuations during electrode biasing experiments on the TJ-II stellarator Paper EX/P4-40
[76] Toi K. *et al* Characteristic features of edge transport barrier formed in helical divertor configuration of the large helical device Paper EX/P1-13
[77] Hughes J.W. *et al* Edge profile stiffness and insensitivity of the density pedestal to neutral fueling in Alcator C-Mod edge transport barriers Paper EX/P3-9
[78] Neudatchin S.V. *et al* ITB-events and their triggers in T-10 and JT-60U Paper EX/P1-8
[79] Ide S. Studies on impact of electron cyclotron wave injection on the internal transport barriers on JT-60U Paper EX/P1-5
[80] Estrada T. *et al* Transitions to improved core electron heat confinement triggered by low order rational magnetic surfaces in the stellarator TJ-II Paper EX/P7-6
[81] Austin M.E. *et al* Transport improvement near low order rational q surfaces in DIII-D Paper EX/P3-1
[82] Ida K. *et al* Dynamic transport study of the plasmas with transport improvement in LHD and JT-60U Paper EX/P4-39
[83] Mantica P. 2006 *Phys Rev. Lett.* **96** 095002
[84] Fujisawa A. *et al* Experimental progress on zonal flow physics in toroidal plasmas Paper OV/4-4
[85] Hoshino K. *et al* Measurement and analysis of the fluctuation s and poloidal flow on JFT-2M tokamak Paper EX/2-2
[86] McKee G.R. *et al* Characterization of zonal flows and their dynamics in the DIII-D tokamak, laboratory plasmas, and simulation Paper EX/2-3
[87] Yan L.W. *et al* Three dimensional identification of zonal flows in the HL-2A tokamak Paper EX/P4-35
[88] Hidalgo C. *et al* On the link between edge momentum redistribution and turbulence in the TJ-II stellerator Paper EX/P7-2
[89] McDonald D.C. *et al* Multi-machine dimensionless transport experiments Paper EX/P3-5
[90] Hennequin P. *et al* Major progress in high spatial and spectral resolution of reflectometry in Tore Supra:density peaking and fluctuation measurements Paper EX/P4-36
[91] Cordey J.G. *et al* 2005 *Nucl. Fusion* **45** 1078
[92] Kaye S.M. *et al* 2006 *Plasma Phys. Control. Fusion* **48** A429
[93] Valovic M. *et al* 2005 *Nucl. Fusion* **45** 942
[94] Stroth U. *et al* 1996 *Nucl. Fusion* **36** 1063
[95] Dinklage A. *et al* Physical model assessment of the energy confinement time scaling in stellarators Paper EX/P7-1
[96] Rice J.E. *et al* Inter-machine comparison of intrinsic toroidal rotation Paper EX/P3-12
[97] Weisen H. *et al* Peaked density profiles in low collisionality H-modes in JET, ASDEX Upgrade and TCV Paper EX/8-4
[98] Zabolotsky A. *et al* Particle and impurity transport in electron-heated discharges in TCV Paper EX/P3-7
[99] Giroud C. *et al* Progress in understanding of impurity transport at JET Paper EX/8-3
[100] Canik J.M. *et al* Reduction of neoclassical transport and observation of a fast electron driven instability with quasisymmetry in HSX Paper EX/5-2
[101] Yokoyama M. *et al* Core electron-root (CERC) confinement in helical plasmas Paper EX/5-3
[102] Sano F. *et al* Configuration studies of Heliotron J Paper EX/5-5Ra